HHS Public Access

Author manuscript

Nature. Author manuscript; available in PMC 2018 February 16.

Published in final edited form as:

Nature. 2017 August 24; 548(7668): 471–475. doi:10.1038/nature23465.

CDK4/6 inhibition triggers anti-tumor immunity

Shom Goel[1,2,*], **Molly J. DeCristo**[3,4,*], **April C. Watt**[1], **Haley BrinJones**[1], **Jaclyn Sceneay**[3,4], **Ben B. Li**[1], **Naveed Khan**[1], **Jessalyn M. Ubellacker**[3,4], **Shaozhen Xie**[1], **Otto Metzger-Filho**[2], **Jeremy Hoog**[5], **Matthew J. Ellis**[6], **Cynthia Ma**[5], **Susanne Ramm**[7,8], **Ian E. Krop**[2], **Eric P. Winer**[2], **Thomas M. Roberts**[1], **Hye-Jung Kim**[9,10,†], **Sandra S. McAllister**[3,4,11,12,†], and **Jean J. Zhao**[1,13,†]

[1]Department of Cancer Biology, Dana-Farber Cancer Institute, Boston MA

[2]Department of Medical Oncology, Dana-Farber Cancer Institute, Boston MA

[3]Department of Medicine, Harvard Medical School, Boston, MA

[4]Hematology Division, Department of Medicine, Brigham and Women's Hospital, Boston MA

[5]Division of Oncology, Department of Internal Medicine, Washington University School of Medicine, St Louis, MO

[6]Lester and Sue Smith Breast Center, Baylor College of Medicine, Houston, TX

[7]Laboratory of Systems Pharmacology, Harvard Program in Therapeutic Science, Harvard Medical School, Boston MA

[8]Renal Division, Department of Medicine, Brigham and Women's Hospital, Boston MA

[9]Department of Cancer Immunology and Virology, Dana-Farber Cancer Institute, Boston, MA

[10]Department of Microbiology and Immunobiology, Division of Immunology, Harvard Medical School, Boston MA

[11]Harvard Stem Cell Institute, Harvard Medical School, Boston MA

Correspondence: Correspondence and requests for materials should be addressed to Shom Goel (shom_goel@dfci.harvard.edu), Sandra McAllister (smcallister1@bwh.harvard.edu), and Jean Zhao (jean_zhao@dfci.harvard.edu).

*These authors contributed equally to this work

†These authors contributed equally to this work

Author Contributions

S.G., M.J.D., H-J. K., S.S.M., and J.J.Z. designed the study. S.G. and M.J.D. performed all experiments with help as follows: A.C.W. and H.B. helped with in vitro tumor cell experiments, qPCR, in vivo treatments, and tumor tissue collection. H-J. K. helped with Treg isolation from mice. J.S. and J.M.U. helped with processing mouse tissues for flow cytometry. N.K. helped with qPCR and COBRA. B.B.L. analyzed mouse transcriptomic data. S.R. conducted digital image analysis. S.X. conducted transcriptomic assays. I.E.K., E.P.W, O.M-F. and T.M.R contributed to scientific discussion that guided the project's direction. M.E., C.M, and J.H. conducted the NeoPalAna trial and provided gene expression data for analysis. S.G. and M.J.D. wrote the paper.

Supplementary Data

Supplementary Information is linked to the online version of the paper at www.nature.com/nature

Competing Financial Interests

Shom Goel has served as a paid scientific advisor to Eli Lilly, and conducts laboratory research funded by Eli Lilly. Eli Lilly did not fund the present study. Matthew Ellis has performed ad hoc consulting for Novartis, Pfizer, and AstraZeneca, receives royalties for PAM50-based diagnostics including Prosigna, and holds stock in Bioclassifier LLC for PAM50-based diagnostics.

[12]Broad Institute of Harvard and MIT, Cambridge MA

[13]Department of Biological Chemistry and Molecular Pharmacology, Harvard Medical School, Boston MA

Abstract

Cyclin-dependent kinases 4 and 6 (CDK4/6) are fundamental drivers of the cell cycle and are required for the initiation and progression of various malignancies[1,2]. Pharmacologic inhibitors of CDK4/6 have shown significant activity against several solid tumors[3,4]. Their primary mechanism of action is thought to be the inhibition of phosphorylation of the retinoblastoma (RB) tumor suppressor, inducing G1 cell cycle arrest in tumor cells[5]. Here, we use murine models of breast carcinoma and other solid tumors to show that selective CDK4/6 inhibitors not only induce tumor cell cycle arrest, but also promote anti-tumor immunity. We confirm this phenomenon through transcriptomic analysis of serial biopsies from a clinical trial of CDK4/6 inhibitor treatment for breast cancer. The enhanced anti-tumor immune response has two underpinnings. First, CDK4/6 inhibitors activate tumor cell expression of endogenous retroviral elements, thus increasing intracellular levels of double-stranded RNA. This in turn stimulates production of type III interferons and hence enhances tumor antigen presentation. Second, CDK4/6 inhibitors markedly suppress the proliferation of regulatory T cells (Tregs). Mechanistically, the effects of CDK4/6 inhibitors on both tumor cells and Tregs are associated with reduced activity of the E2F target, DNA methyltransferase 1. Ultimately, these events promote cytotoxic T cell-mediated clearance of tumor cells, which is further enhanced by the addition of immune checkpoint blockade. Our findings indicate that CDK4/6 inhibitors increase tumor immunogenicity and provide rationale for new combination regimens comprising CDK4/6 inhibitors and immunotherapies as anti-cancer treatment.

We first assessed the impact of CDK4/6 inhibition *in vivo* using our recently described *MMTV-rtTA/tetO-HER2* transgenic mouse model of mammary carcinoma[6]. Cells derived from these tumors express RB and arrest in response to CDK4/6 inhibition[6]. In three independent experiments, the CDK4/6 inhibitor abemaciclib caused regression of bulky tumors, evidenced by a ~40% reduction in tumor volume at the 12-day end-point (Fig. 1a). As expected, abemaciclib reduced tumor cell proliferation (Extended Data Fig. 1a). Expression analysis across a panel of 3,826 cancer-related genes from *MMTV-rtTA/tetO-HER2* tumors (Fig. 1b) showed that abemaciclib downregulated genes within Gene Ontology (GO) and Gene Set Enrichment Analysis (GSEA) terms relating to cell cycle, mitosis, and E2F targets (Extended Data Fig. 1b–d). Strikingly, only two GO process terms were significantly enriched for genes upregulated by abemaciclib: “antigen processing and presentation of peptide antigen” and “antigen processing and presentation” (Fig. 1c). Specifically, genes encoding murine major histocompatibility complex (MHC) class I molecules were upregulated in abemaciclib-treated tumors (*H2d1, H2k1,* and *B2m*), as were genes directing peptide cleavage (*Erap1*), peptide transporters (*Tap1* and *Tap2*), and transporter-MHC interactions (*Tapbp)* (Fig. 1d). Moreover, abemaciclib treatment *in vitro* increased expression of homologous genes in human breast cancer cell lines (MDA-MB-453, MCF7, and MDA-MB-361) (Fig. 1e; Extended Data Fig. 2a) and palbociclib, another CDK4/6 inhibitor, yielded similar results (Extended Data Fig. 2b). Importantly,

treatment with either agent increased cell-surface expression of β2M and MHC class I proteins (Extended Data Fig. 2c). The CDK4/6 inhibitor-induced increase in expression of antigen processing and presentation genes was also observed in a patient-derived breast cancer xenograft of a treatment-refractory breast cancer (PDX 14-07, previously described[6]) (Fig. 1f). Furthermore, analysis of The Cancer Genome Atlas (TCGA) data[7] revealed that breast cancers harboring cyclin D1 amplification (i.e., enhanced CDK4/6 activity) display significantly lower expression of *HLA-A, HLA-B,* and *HLA-C* than non-amplified tumors (Extended Data Fig. 2d).

To determine the functional consequences of increased antigen presentation gene expression, we treated ovalbumin (OVA) expressing murine cancer cell lines (*MMTV-PyMT*-S2WTP3-OVA and B16-OVA) with abemaciclib. Abemaciclib increased expression of MHC class I-bound SIINFEKL, an 8 amino acid peptide derived from OVA (Extended Data Fig. 2e), confirming enhanced antigen processing and presentation. Co-culture of abemaciclib-pretreated tumor cells with MHC class I-restricted OVA-specific $CD8^+$ T cells (OT-I cells) significantly increased OT-I cell proliferation, IFN-gamma production, and TNF-alpha production (Fig. 1g; Extended Data Figs. 2f, g). $CD8^+$ T cell proliferation was both antigen-specific (P14 $CD8^+$ T cells, which recognize an irrelevant antigen, did not increase their proliferation) and MHC class I-specific (MHC class I blocking antibody partially suppressed OT-I T cell proliferation) (Fig. 1g; Extended Data Fig. 2f).

In agreement with other reports[2,6], abemaciclib did not directly induce breast cancer cell apoptosis; rather, it caused cell cycle arrest and induced cellular phenotypes consistent with senescence (Extended Data Fig. 3a, b). Cellular senescence has been associated with apoptosis resistance[8]; indeed, abemaciclib reduced tumor cell Poly ADP-ribose polymerase cleavage and suppressed the apoptotic response to staurosporine (Extended Data Fig. 3c, d). Collectively, these results establish that CDK4/6 inhibitors induce breast cancer cell cytostasis without directly causing their apoptosis, and enhance their capacity to present antigen and stimulate cytotoxic T cells.

We next sought mechanistic insight for the increase in antigen presentation after CDK4/6 inhibition. Genome-wide transcriptomic analysis of three human breast cancer cell lines and PDX 14-07 tumors revealed that abemaciclib upregulated expression of genes within GO terms related to interferon signaling and cellular defense response to virus (Fig. 2a, b; Extended Data Fig. 4a). Several interferon-sensitive transcription factors (e.g., *STAT1, STAT2, IRF2, IRF6, IRF9,* and *NLRC5*) were upregulated in all three cell lines, PDX 14-07 tumors, and *MMTV-PyMT*-S2WTP3 cells (Figs. 2c, d; Extended Data Figs. 4b, c). Similar trends were observed when abemaciclib was given in conjunction with anti-estrogen therapy - the current standard in luminal breast cancer treatment (Extended Data Fig. 4d). Expression of other interferon-sensitive genes (ISGs) - *OAS1, OAS2, IFIT1, IFIT2, BST2, SP100, RSAD2* - was also enhanced in cell lines and PDX tumors, suggesting global upregulation of an interferon-driven transcriptional program (Extended Data Figs. 4e, f). Consistent with active interferon signaling, both phosphorylated and total STAT1 protein were increased after abemaciclib treatment (Extended Data Fig. 4g). Furthermore, forced overexpression of the endogenous CDK4/6 inhibitor *CDKN2A* (encoding $p16^{INK4a}$)

increased expression of *STAT1, B2M,* and MHC class I genes (Extended Data Fig. 4h), suggesting that these are "on-target" effects.

Importantly, we made similar observations in *MMTV-rtTA/tetO-HER2* tumor tissues after abemaciclib treatment. Enriched GSEA expression signatures included "allograft rejection", "interferon alpha response", and "interferon gamma response" (Fig. 2e). Specifically, abemaciclib also significantly increased tumor expression of interferon-responsive transcription factors in these tumors (Fig. 2f), as well as that of interferon-inducible T cell chemoattractants and other ISGs involved in lymphocyte adhesion and co-stimulation (Extended Data Figs. 4i, j). STAT1 protein levels were also higher within tumor cells of the abemaciclib-treated cohort (Fig. 2g). In keeping with their roles in regulating antigen presentation via MHC class I, *in vivo* expression of transcription factors *Stat1* and *Nlrc5* was tightly correlated with that of *H2d1, H2k1, Tap1, Tap2,* and *Tapbp* in *MMTV-rtTA/tetO-HER2* tumors (Extended Data Fig. 4k). Thus, CDK4/6 inhibition directly induces ISG expression in tumor cells, likely explaining their enhanced capacity for antigen presentation.

We next interrogated genome-wide expression data from the NeoPalAna trial, in which patients with primary ER-positive breast cancer underwent tumor biopsies before commencing palbociclib and serially after 2 and 12 weeks of treatment (Extended Data Fig. 5a)[9]. As expected, palbociclib treatment significantly downregulated genes within the "E2F target" and other cell cycle-related signatures (Extended Data Fig. 5b). When we compared upregulated genes from biopsies taken before initiation of palbociclib to those after 12 weeks of treatment, 3 of the top 5 ranked "Hallmarks" GSEA signatures were "allograft rejection", "inflammatory response" and "interferon gamma response" (Fig. 2h) and these gene sets were already significantly upregulated after 2 weeks of palbociclib treatment (Extended Data Fig. 5c). These signatures are the same as those we observed to be upregulated in the tumors from abemaciclib-treated *MMTV-rtTA/tetO-HER2* mice (Fig. 2e), and demonstrate the clinical relevance of our findings.

We speculated that heightened ISG expression after CDK4/6 inhibition might be caused by enhanced tumor cell interferon production. The Janus Kinases (JAKs) mediate intracellular signaling after ligand-dependent activation of interferon receptor, and the JAK inhibitor ruxolitinib completely mitigated abemaciclib-induced increases in tumor cell p-STAT1 and total STAT1 (Extended Data Fig. 6a), suggesting that CDK4/6 inhibition stimulates tumor cell interferon production. Notably, ELISA did not detect interferons alpha, beta, or gamma in conditioned medium of abemaciclib-treated tumor cells (not shown), and neutralizing antibodies against interferons alpha and gamma did not mitigate interferon signaling (Extended Data Fig. 6b–d). However, gene expression and protein secretion of type III interferons (IL-29, IL-28a, and IL-28b) were significantly increased in abemaciclib-treated tumor cells (Fig. 3a; Extended Data Figs. 6e, f). Neutralizing antibodies to type III interferons reversed abemaciclib-induced increases in tumor cell p-STAT1 and total STAT1 (Fig. 3b). Collectively, these data suggest that CDK4/6 inhibition increases tumor cell production of type III interferons to drive ISG expression in an autocrine fashion.

Increased tumor cell interferon signaling via type III interferon production has previously been shown to occur in response to DNA demethylation caused by agents such as 5-

azacytidine, which inhibits DNA methyltransferases (DNMTs)[10]. In that context, DNMT inhibition reduces methylation of endogenous retroviral genes (ERVs), triggering "viral mimicry" and a double-stranded RNA (dsRNA) response, in turn stimulating type III interferon production to activate ISGs[10]. Notably, the mammalian DNA methyltransferase *DNMT1* is a bona fide E2F target gene, and CDK4/6 enzyme activity can enhance DNMT1 gene expression in an RB-E2F dependent fashion[11]. Strikingly, tumor cell levels of *DNMT1* (but not *DNMT3A*) mRNA and protein fell markedly and rapidly in abemaciclib-treated cell lines (Fig. 3c; Extended Data Figs. 7a–c). Similarly, abemaciclib reduced *DNMT1* mRNA levels *in vivo* in both PDX 14-07 and *MMTV-rtTA/tetO-HER2* tumors (Fig. 3d; Extended Data Fig. 7d). These were on-target effects, as abemaciclib did not reduce *DNMT1* levels in tumor cells expressing shRNA targeting *RB1* (Extended Data Fig. 7e). The abemaciclib-related increases in *IFNL2, STAT1*, and *HLA-B* expression were also mitigated in shRNA-*RB1* cells (Extended Data Fig. 7e), supporting the concept that the RB-E2F-DNMT1 axis mediates type III interferon production and its downstream consequences.

Consistent with previous studies[10,12], suppression of *DNMT1* was associated with reduced DNA methylation at ERV sequences; combined bisulfite restriction analysis (COBRA) showed that abemaciclib decreased tumor cell DNA methylation at the 5′-LTR of *ERV3-1* (Extended Data Fig. 7f). Accordingly, expression of certain ERVs was increased *in vitro* and *in vivo* (Fig. 3e, f; Extended Data Fig. 7g), accompanied by significantly higher levels of dsRNA within tumor cells (Fig. 3g; Extended Data Fig. 7h). In turn, expression of the dsRNA pattern recognition receptors, RIG-1 (*DDX58*), LGP2 (*DHX58*), and MDA5 (*IFIH1*), was significantly increased in cell lines and PDX tumors (Extended Data Fig. 7i, j). In further support of abemaciclib-mediated *DNMT1* suppression as the trigger for this cascade of events, overexpression of *DNMT1* in tumor cells attenuated the abemaciclib-induced increase in expression of dsRNA response genes, type III interferon, and ISGs (Fig. 3h; Extended Data Fig. 7k). Independent of altered ERV expression, CDK4/6 inhibitors could theoretically increase tumor cell immunogenicity by inducing a "senescence associated secretory phenotype" (SASP)[13]. Although abemaciclib increased tumor cell beta-galactosidase activity (Extended Data Fig. 3b, 8a), expression of key SASP factors was not increased (Extended Data Fig. 8b, c and Supplementary Table 1). In contrast, doxorubicin increased tumor cell expression of SASP genes (Extended Data Fig. 8d), consistent with the notion that the SASP is more pertinent to DNA damage response-associated senescence[13] and does not explain tumor immunogenicity after CDK4/6 inhibition.

Our observation that CDK4/6 inhibition enhances the efficiency of tumor cell antigen presentation prompted us to examine the tumor immune microenvironment. Flow cytometric analysis of *MMTV-rtTA/tetO-HER2* tumors revealed that abemaciclib did not alter fractions of most types of tumor-infiltrating leukocytes (Extended Data Fig. 9a). Strikingly, however, there were significant increases in $CD3^+$ T cells (Fig. 4a) and reductions in $CD4^+FOXP3^+$ regulatory T cells (Tregs, Fig. 4b). Circulating Treg numbers were also significantly lower (Extended Data Fig. 9b). These results were upheld in *MMTV-PyMT* mammary and CT-26 colorectal carcinomas (Extended Data Fig. 9c, d). Moreover, the Treg:CD8 T cell ratio decreased significantly in abemaciclib-treated tumors, further suggesting a tipping of the immune balance in favor of anti-tumor immunity (Fig. 4c).

In tumor-free mice, both abemaciclib and palbociclib significantly reduced Treg numbers and the Treg:CD8 ratio in the spleen and lymph nodes, demonstrating tumor-independent effects of these agents (Fig. 4d; Extended Data Fig. 9e, f). Plasma levels of anti-nuclear and anti-double stranded DNA antibodies were unchanged (not shown; Extended Data Fig. 9g), indicating no significant accompanying autoimmune phenotype. To understand why Tregs were reduced in number, we analyzed the impact of CDK4/6 inhibitors on various aspects of Treg biology. Palbociclib and abemaciclib each significantly reduced total thymic mass, decreased immature $CD4^+CD8^+$ double-positive thymocytes, and increased the fractions of $CD4^+$ and $CD8^+$ single-positive thymocytes (Extended Data Fig. 9h–k), consistent with previous reports of CDK6 inhibition[14]. However, proportions of thymic Tregs were unchanged, arguing against a defect in natural Treg production (Extended Data Fig. 9l). Similarly, CDK4/6 inhibitors did not prevent *in vitro* differentiation of naïve $CD4^+$ T cells into Tregs, and did not affect rates of Treg apoptosis (Extended Data Fig. 9m, n). We then turned our attention to Treg proliferation. *In vitro*, abemaciclib markedly reduced the proliferation of $CD4^+CD25^+$ Tregs isolated from spleens and lymph nodes of wild-type mice, but had a weaker effect on the proliferation of $CD4^+CD25^-$ and $CD8^+$ T cells (Fig. 4e). Likewise, the fraction of proliferating Tregs, but not $CD8^+$ T cells, within abemaciclib-treated tumor tissue was significantly reduced (Fig. 4f; Extended Data Fig. 9o). DNMT1 inhibition in Tregs has previously been reported to suppress their proliferation, ostensibly via hypomethylation of the *Cdkn1a* promoter, thus increasing expression of the *Cdkn1a* protein, p21 - a potent and promiscuous cell cycle inhibitor[15]. In tumor-free mice treated with abemaciclib for 12 days, *Dnmt1* expression was reduced in Tregs by ~70%; in contrast, *Dnmt1* mRNA was unchanged in naïve $CD4^+$ T cells and fell by only 20% in $CD8^+$ T cells (Extended Data Fig. 9p). Mirroring the magnitude of these changes, expression of *Cdkn1a* increased 75-fold in Tregs, 2.8-fold in $CD8^+$ T cells, and was unchanged in naïve $CD4^+$ T cells (Extended Data Fig. 9q). Therefore, the relatively selective suppression of Treg proliferation after CDK4/6 inhibition could relate to enhanced cell cycle inhibition due to overexpression of p21, associated with reduced levels of DNMT1.

Tumor cells presenting antigen via MHC class I can be recognized by cytotoxic T lymphocytes (CTLs), and Tregs suppress CTL responses, in part by promoting their exhaustion[16]. Therefore, to determine whether CTLs were involved in abemaciclib-mediated therapeutic efficacy, we implanted *MMTV-rtTA/tetO-HER2* tumor fragments orthotopically into athymic $Foxn1^{nu}$ mice maintained on doxycycline, and treated them once tumors were established. In contrast to tumors in immunocompetent mice, abemaciclib-treated tumors in nude mice continued to grow, albeit at a significantly slower rate than vehicle-treated tumors, and in no case did tumors regress (Extended Data Fig. 10a, b). We therefore treated *MMTV-rtTA/tetO-HER2* tumor-bearing mice with an anti-CD8 antibody prior to abemaciclib administration. Abemaciclib-induced tumor regression, which was observed in control IgG treated mice, was significantly mitigated by CD8 neutralization (Fig. 4g and Extended Data Fig. 10c). Hence, tumor regression mediated by CDK4/6 inhibition is, at least in part, dependent on the presence of CTLs.

Intratumoral $CD8^+$ T cells in abemaciclib-treated mice displayed markedly reduced expression of PD-1, Tim-3, CTLA-4, and LAG3 (Fig. 4h and Extended Data Fig. 10d–g), markers typically indicative of T cell exhaustion[17]. The number of inhibitory receptors

detected on any given CTL was lower in abemaciclib-treated *MMTV-rtTA/tetO-HER2* and *MMTV-PyMT* tumors (Fig. 4i, Extended Data Fig. 10h). Specifically, the fractions of both PD-1^{high} and PD-1^{+}/TIM-3^{+} CTLs were significantly reduced (Fig. 4h; Extended Data Fig. 10d). Levels of *Ifng* mRNA (the main effector cytokine of CTLs) were more than 4-fold higher in abemaciclib-treated bulk tumor tissues (Extended Data Fig. 10i). Collectively, these results indicated that CDK4/6 inhibition results in activation of CTLs, which are necessary for abemaciclib-induced tumor regression.

Increased tumor cell antigen presentation coupled with anti-tumor T cell responses suggested that immune checkpoint blockade might further enhance the efficacy of abemaciclib. We treated *MMTV-rtTA/tetO-HER2* tumor-bearing mice with either vehicle or abemaciclib, and a control IgG or an anti-PDL1 antibody (Extended Data Fig. 10j). In agreement with our initial experiments, abemaciclib-treated tumors initially decreased in volume before stabilizing and ultimately resuming growth by day 21 (Fig. 4j). In contrast, tumors in mice treated with abemaciclib and anti-PDL1 combination therapy regressed to the greatest degree (~70% reduction in tumor volume by day 13), and did not resume growth by day 35 (Fig. 4j; Extended Data Fig. 10k). Similar results were obtained for the CT-26 colorectal carcinoma model, wherein combination therapy induced complete tumor regression in all cases, and rendered mice disease-resistant when re-challenged with a subsequent injection of CT-26 tumor cells 5 weeks after stopping therapy (Extended Data Fig. 10l, m).

Collectively, our data in cell lines, animal models, and breast cancer patients demonstrate that CDK4/6 inhibitors enhance anti-tumor immunity by overcoming two central mechanisms of tumor immune evasion (Extended Data Fig. 10n). First, they increase tumor cells' functional capacity to present antigen. Second, they reduce the immunosuppressive Treg population by suppressing their proliferation. Intriguingly, these phenomena might not only cooperate to enhance tumor immunogenicity, but could also have the same mechanistic underpinning – suppression of the Rb-E2F axis, leading to reduced *DNMT1* expression and thus hypomethylation of genes that regulate immune function[10,12,15]. The selective suppression of Treg proliferation (and not that of CD8^{+} or naïve CD4^{+} T cells) might relate to the fact that Tregs express higher levels of *Rb1*, a key mediator of CDK4/6 pathway modulation[18] (e.g. *Rb1* expression is 3.1-fold higher in Tregs than CD8^{+} T cells[19]). With respect to breast cancer specifically, we note that the majority of human breast cancers are estrogen-receptor positive – these tumors generally retain Rb function and are considered inherently less immunogenic. Interestingly, a high number of Tregs in these tumors also predicts a poor clinical outcome[20]. Our findings therefore suggest that CDK4/6 inhibitors might enhance the susceptibility of such tumors to immune checkpoint blockade.

Methods

Animal experiments

MMTV-rtTA/tetO-HER2 mice[6] were maintained in house. Female FVB *MMTV-PyMT*, Balb/c (6–7 weeks old), and *Foxn1^{nu}* (8 weeks old) mice were purchased from Jackson Labs. Female FVB mice (7 weeks old) were purchased from Taconic Biosciences. P14-TCR transgenic mice (gift from Dr. Kai Wucherpfennig, Harvard Medical School), and OT-I mice

(C57BL/6 Tg(TcraTcrb)1100Mjb/J; Jackson Labs) were used as a source of $CD8^+$ T cells for in vitro co-culture assays. FVB $CD45.2^+$ mice (gift from Dr. Daniel Tenen, Harvard Medical School) were used as a source of T cells for in vitro studies.

Tumors were induced and maintained in *MMTV-rtTA/tetO-HER2* mice using doxycycline as previously described[6]. For experiments in transgenic *MMTV-rtTA/tetO-HER2* and *MMTV-PyMT* mice, tumors measured 4–10 mm at treatment initiation. Prior to treatment, mice were assigned into groups of equal average tumor volume. For CT-26 experiments, 1×10^5 tumor cells were injected subcutaneously in 1:1 PBS:Matrigel, injected subcutaneously into Balb/c mice, and treatment was initiated one week later. For rechallenge experiments, 5×10^5 tumor cells were injected subcutaneously in 1:1 PBS:Matrigel 33 days after treatment was stopped. PDX 14-07 was established from a biopsy of a liver metastasis from a patient with ER+/Her2+ breast cancer as previously described[6].

For studies in *Foxn1^{nu}* mice, *MMTV-rtTA/tetO-HER2* tumor fragments were orthotopically implanted bilaterally into nude mice, as previously described[6]. Prior to treatment initiation, mice were randomized into groups of equal average tumor volume (5–10 mm diameter).

For *in vivo* experiments, samples sizes were determined based on previous model-specific experience. Tumors were measured by caliper 2–3 times per week, and volume was calculated as previously described[6]. For tumor growth kinetic analysis, we performed two-way ANOVA or one-way ANOVA tests with correction for multiple comparisons using Sidak's multiple comparisons test. No animals were excluded from analyses. *Ex vivo* analyses of mouse tissues were performed in a blinded fashion such that the investigators were unaware of treatment groups. Source data for tumor volume measurements can be found in Supplementary Table 2.

Abemaciclib (75–90 mg/kg, as noted for individual experiments, Haoyuan Chemexpress, prepared as previously described[6]) and palbociclib (90mg/kg, Haoyuan Chemexpress, diluted in 50 nM sodium D-lactate) were administered daily by oral gavage. For CD8 depletion experiments, mice were injected intraperitoneally with either α-CD8 antibody (400 μg; clone YTS 169.4, BioXcell) or isotype control (400 μg; clone LTF-2, BioXcell) 48 and 24 hours prior to beginning abemaciclib therapy (90mg/kg) and every 4 days thereafter. For combination therapy, treatment with abemaciclib was initiated at a dose of 90 mg/kg daily for 3 days; thereafter, the dose was dropped to 75mg/kg daily and intraperitoneal injection of either α-PDL1 antibody (200 μg every 72 hours; BioXcell, clone 10F.9G2) or isotype control antibody (200 μg every 72 hours, clone LTF-2, BioXcell) was added to the regimen.

Mice were euthanized using CO_2 inhalation. All mouse experiments were performed in compliance with federal laws and institutional guidelines as approved by the Institutional Animal Care and Use Committees of Dana-Farber Cancer Institute, Harvard Medical School, and Boston Children's Hospital. The maximum tumor diameter permitted under the relevant animal protocols is 25mm, and this limit was not exceeded in any experiment.

Immunohistochemistry and immunofluorescence

Immunostaining for Ki-67 (Vector), HER2 (AB16901; Abcam), and STAT1 (AB47425; Abcam) was performed as previously described[6]. Secondary antibodies (AF488 AffiniPure donkey anti-mouse IgG, Cy3 AffiniPure donkey anti-rabbit IgG) were from Jackson ImmunoResearch Laboratories. Images were acquired with a Yokogawa spinning disk confocal on an inverted Nikon T*i* fluorescence microscope using MetaMorph image acquisition software, and 3–5 fields were analyzed per tumor. Image analysis was performed using a semi-automated in-house platform (NIH ImageJ).

Immunofluorescence for FoxP3 (clone FJK-16s; eBioscience), CD8 (clone 4SM15; eBioscience), and Ki-67 (clone SP6; Thermo Scientific) was performed as previously described[21]. Secondary antibodies (AF488 donkey anti-rabbit IgG, AF647 goat anti-rat IgG) were from Life Technologies. Tissues were counterstained with DAPI (Invitrogen). Images were acquired on a Nikon Eclipse N*i* microscope using NIS Elements software, and 5–10 fields were analyzed per tumor.

Human cell lines

BT474, SKBR3, MDA-MB-361, MDA-MB-453, and MCF7 human breast cancer cell lines were maintained as previously described[6] with slight modifications: antibiotics and anti-fungals were not used in cell culture media. MCF7 cells were cultured in RPMI medium (Gibco) supplemented with 10% FBS (Gibco). All cell lines were obtained from ATCC, tested negative for mycoplasma, and their identity was verified by short tandem repeat analysis (Promega GenePrint 10 System).

Murine cell lines

MMTV-PyMT-S2WTP3 cells[22] (gift from Dr. Andreas Möller, QIMR Berghofer Medical Research Institute) were cultured in DMEM (Gibco) supplemented with 10% FBS (Gibco). B16-OVA cells[23] were cultured in DMEM supplemented with 10% FBS and 250 μg/mL G418 (Invitrogen). CT-26 cells (gift from Dr. Steve Elledge, Harvard University) were cultured in RPMI (Gibco) supplemented with 10% FBS. All cell lines tested negative for mycoplasma, and their murine strain of origin was confirmed by short tandem repeat analysis (Bioassay Methods Group, NIST).

In vitro drug studies

Abemaciclib and lapatinib (Haoyuan Chemexpress) were diluted as previously described[6]. For in vitro use, palbociclib was diluted in DMSO. Cleaved PARP was measured after 48 hours of treatment with DMSO, lapatinib, or abemaciclib. Lapatinib was used at 30 nM for BT474 and SKBR3; 500 nM for MDA-MB-453 and MDA-MB-361. Abemaciclib was used at 300 nM for BT474 and SKBR3; 25 nM for MDA-MB-453; 500 nM for MDA-MB-361. For staurosporine experiments, MDA-MB-453 cells were pretreated with DMSO or abemaciclib (500 nM) for 0, 1, or 7 days prior to exposure to staurosporine (500nM, Enzo Life Sciences) for 4 hours. For hormonal therapy studies, cells were treated with combinations of DMSO, abemaciclib (100 nM), and fulvestrant (100 nM, Sigma Aldrich). To determine JAK dependency, cells were treated with combinations of DMSO, abemaciclib (500nM), and ruxolitinib (500nM, Selleckchem) for 7 days.

Western blots

Western blotting was carried out as previously described[6] using antibodies to cleaved PARP (CST 9541), cleaved caspase-3 (CST 9661), phospho-STAT1 Y701 (CST 9167), STAT1 (CST 9172), and FLAG (CST 2368) (Cell Signaling Technologies), vinculin (V9131, Sigma) and DNMT1 (92314, Abcam). For western blots assessing phosphorylated and total STAT1 in tumor cells, lysates from equivalent numbers of cells were loaded in each lane. Uncropped western blots can be found in Supplementary Figure 1.

β-galactosidase activity

SA-β-galactosidase expression was determined as previously described[6].

Transcriptome methodology

AmpliSeq™ libraries were constructed and sequenced on the Ion Torrent Proton platform (Thermo Fisher) according to the manufacturer's instructions as previously described[24,25]. For human gene analysis in cell lines, the Ion AmpliSeq Transcriptome Human Gene Expression Kit is designed for targeted amplification of over 20,000 human RefSeq genes simultaneously in a single primer pool. A short amplicon (~110 bp) is amplified for each targeted gene. Since an AmpliSeq transcriptome mouse kit is not commercially available, an Ion AmpliSeq™ Custom Panel was designed by the manufacturer (Thermo Fisher) using Ion AmpliSeq™ Designer for targeted amplification of 3,826 mouse genes that are most relevant for our studies (one short amplicon for each gene) in one primer pool for mouse studies. For each sample, 10 ng of total RNA was used for cDNA library preparation. Multiple libraries were multiplexed and clonally amplified using the Ion OneTouch 2 System (Thermo Fisher), and then sequenced on an Ion Torrent Proton machine (Thermo Fisher). Data was first analyzed by Torrent Suite and ampliSeqRNA analysis plugin (Thermo Fisher) to generate count data.

Mouse transcriptome analysis

Raw read counts per gene were mapped to corresponding human homologs, using homology information from the Mouse Genome Informatics database (The Jackson Laboratory). For GO analysis, differential gene expression was determined using DESeq2[26] and genes were ranked according to log2 fold change (MAP). For GSEA analysis, we used the GSEAPreranked tool, with the above ranked gene list, using MSigDB v5.1 Hallmarks gene sets collection and the "classic" method for calculating enrichment scores[27,28].

Human transcriptome analysis

Analyses were performed on normalized read counts per gene. For GO analysis, only genes with an absolute read count of >20 on at least one sample were included. For these genes, the fold change in normalized read count was determined for each replicate experiment, and the mean fold change was calculated for each gene. Genes with a mean fold change of >2 (DMSO vs abemaciclib) were then included for analysis using gene ontology enrichment analysis.

The Cancer Genome Atlas (TCGA) analysis

Gene expression data were obtained using the cBioPortal for Cancer Genomics (http://www.cbioportal.org). Data were obtained from the breast cancer dataset "TCGA, Provisional (1105 samples)" for comparisons between cyclin D1 shallow deletion, amplified, gain, and diploid tumors[7,29].

RT-qPCR

RT-qPCR was performed as previously described[6]. Primer sequences used for qPCR were as follows: *Ifng* (mouse) forward:5′-ATG-AAC-GCT-ACA-CAC-TGC-ATC-3′; reverse:5′-CCA-TCC-TTT-TGC-CAG-TTC-CTC-3′. *Tap1* (mouse) forward:5′-GGA-CTT-GCC–TTG-TTC-CGA-GAG-3′; reverse:5′-GCT-GCC-ACA-TAA-CTG-ATA-GCG-A-3′. *Tap2* (mouse) forward:5′-CTG-GCG-GAC-ATG-GCT-TTA-CTT-3′; reverse:5′-CTC-CCA-CTT-TTA-GCA-GTC-CCC-3′. *Tapbp* (mouse) forward:5′-GGC-CTG-TCT-AAG-AAA-CCT-GCC-3′; reverse:5′-CCA-CCT-TGA-AGT-ATA-GCT-TTG-GG-3′. *Erap1* (mouse) forward: 5′-TAA-TGG-AGA-CTC-ATT-CCC-TTG-GA-3′; reverse:5′-AAA-GTC-AGA-GTG-CTG-AGG-TTT-G-3′. *Nlrc5* (mouse) forward:5′-GCT-GAG-AGC-ATC-CGA-CTG-AAC-3′; reverse:5′-AGG-TAC-ATC-AAG-CTC-GAA-GCA-3′. *Il6* (mouse) forward:5′-TAG-TCC-TTC-CTA-CCC-CAA-TTT-CC-3′; reverse:5′-TTG-GTC-CTT-AGC-CAC-TCC-TTC-3′. *Dnmt1* (mouse) forward:5′-CCG-TGG-CTA-CGA-GGA-GAAC-3′; reverse:5′-TTG-GGT-TTC-CGT-TTA-GTG-GGG-3′. *Cdkn1a* (mouse) forward:5′-CCT-GGT-GAT-GTC-CGA-CCT-G-3′; reverse:5′-CCA-TGA-GCG-CAT-CGC-AAT C-3′. *B2M* (human) forward:5′-GAG-GCT-ATC-CAG-CGT-ACT-CCA-3′; reverse:5′-CGG-CAG-GCA-TAC-TCA-TCT-TTT-3′. *HLA-A* (human) forward:5′-ACC-CTC-GTC-CTG-CTA-CTC-TC-3′; reverse:5′-CTG-TCT-CCT-CGT-CCC-AAT-ACT-3′. *HLA-B* (human) forward:5′-CAG-TTC-GTG-AGG-TTC-GAC-AG-3′; reverse:5′-CAG-CCG-TAC-ATG-CTC-TGG-A-3′. *HLA-C* (human) forward:5′-GGA-CAA-GAG-CAG-AGA-TAC-ACG-3′; reverse:5′-CAA-GGA-CAG-CTA-GGA-CAA-CC-3′. *STAT1* (human) forward:5′-CAG-CTT-GAC-TCA-AAA-TTC-CTG-GA-3′; reverse:5′-TGA-AGA-TTA-CGC-TTG-CTT-TTC-CT-3′. *IL6* (human) forward:5′-ACT-CAC-CTC-TTC-AGA-ACG-AAT-TG-3′; reverse:5′-CCA-TCT-TTG-GAA-GGT-TCA-GGT-TG-3′. *IFNL2* (human) forward:5′-ACG-CGA-GAC-CTG-AAT-TGT-GT-3′; reverse:5′-AGC-GAC-TGG-GTG-GCA-ATA-AA-3′. *DDX58* (human) forward:5′-CTG-GAC-CCT-ACC-TAC-ATC-CTG-3′; reverse:5′-GGC-ATC-CAA-AAA-GCC-ACG-G-3′. *DHX58* (human) forward:5′-GGG-CCT-CCA-AAC-TCG-ATG-G-3′; reverse:5′-TTC-TGG-GGT-GAC-ATG-ATG-CAC-3′. *OAS2* (human) forward:5′-GGA-GCT-TCC-TGA-TTG-GCA-GA-3′; reverse:5′—ATG-TAG-GGT GGC-AAG-CAC-TG-3′. *RB1* (human) forward:5′-CTC-TCG-TCA-GGC-TTG-AGT-TTG-3′; reverse:5′-GAC-ATC-TCA-TCT-AGG-TCA-ACT-GC-3′. Relative copy number was determined by calculating the fold change difference in the gene of interest relative to *GAPDH* or *HSP90AB1* (human), or *Actb or Hsp90ab1* (mouse). qPCR was performed on the Applied Biosystems 7300 machine.

Flow cytometry

Tumor cell lines: 1×10^6 cells per condition were stained with the appropriate antibodies diluted in PBS (Hyclone) plus 2% FBS (Life Technologies) for 30 minutes on ice. Matched fluorescence minus one (FMO) staining for each condition was performed as a control.

Blood: Obtained by retro-orbital sampling at intermediate time points and by cardiac puncture at experimental endpoints. Blood cells and plasma were separated by centrifugation at 1,500 × g for 8 minutes at 4°C.

Spleen, thymus, and lymph nodes: Single cell suspensions were obtained by mechanical digestion.

Tumor: Tumors were first mechanically disrupted by chopping, then chemically digested in dissociation buffer (2 mg/mL collagenase type IV (Worthington Biochemical), 0.02 mg/mL DNase (Sigma Aldrich) in DMEM (Life Technologies) containing 5% FBS (Life Technologies), PenStrep (Hyclone)) with agitation at 37°C for 45 minutes.

Following RBC lysis if necessary (blood, spleen, thymus, tumor; PharmLyse, BD Biosciences), single cell suspensions were blocked with anti-CD16/32 (Biolegend) for 20 minutes on ice and then incubated with appropriate antibodies for 30 min on ice.

Murine antibodies: Antibodies were purchased from Biolegend unless otherwise indicated: CD45 (clone 30-F11), CD3 (clone 145-2C11), CD8 (clone 53-6.7), CD4 (clone RM4-5), PD-1 (clone 29F.1A12), Tim-3 (clone RMT3-23), CTLA-4 (clone UC10-4B9), LAG-3 (clone C9B7W), B220 (clone RA3-6B2), NK1.1 (clone PK136), CD11b (clone M1/70), Ly6G (clone 1A8), Ly6C (clone AL-21; BD Pharmigen), and FoxP3 (clone FJK-16s; eBioscience). Human antibodies: β2-microglobulin (clone 2M2) and HLA-A,B,C (clone W6/32). Anti-mouse/rat FoxP3 staining set (eBioscience) was used for intracellular staining according to the manufacturer's instructions. dsRNA was detected by the K1 antibody (English and Scientific Consulting (Hungary) using 75% ethanol for fixation. 7AAD was used to distinguish live/dead cells, except in cases requiring intracellular staining in which case eFluor 450 (eBioscience) or Zombie Yellow (Biolegend) fixable viability dyes were used. To determine the absolute number of cells in a sample, CountBright absolute counting beads (Molecular Probes, ThermoFisher) were added. Flow cytometry was performed on a LSRII (BD Biosciences) or FACSCANTOII (BD Biosciences), and data was analyzed using FlowJo (TreeStar). Flow cytometry gating strategies can be found in the Supplementary Methods (regulatory T cell gating strategy, Supplementary Methods 1; thymic cell populations, Supplementary Methods 2; and immune checkpoint molecules on intratumoral T cells, Supplementary Methods 3).

Tumor cell/OT-I co-culture assay

MMTV-PyMT-S2WTP3-OVA and B16-OVA cells were pre-treated with abemaciclib (500 nM or 1000 nM, respectively) or DMSO for 7d. Tumor cells were pre-incubated with 40 μg/mL of appropriate antibodies for 1 hr at 37°C. For the *MMTV-PyMT*-S2WTP3-OVA experiments, anti-H-$2K^b$ (clone Y-3) or isotype control IgG2b (clone MPC-11) were used

from Bioxcell. For the B16-OVA experiments, anti-H-2K^b-SIINFEKL (clone 25-D1.16) or isotype control (clone IS5-21F5) from Miltenyl Biotec were utilized. CD8+ T cells were isolated from spleens and lymph nodes of OT-I or P14 mice using a CD8a+ T cell isolation kit (Miltenyl Biotec) with an autoMACS pro separator. Isolated T cells were suspended in RPMI (ATCC) with 5% FBS, labeled with 5 μM CFSE (Biolegend) for 10 minutes in the dark at room temperature, and washed twice in 10× volume of T cell media (RPMI, 10% FBS, 55 μM 2-Mercaptoethanol (Gibco)). 1×10^5 CD8$^+$ T cells were co-cultured with abemaciclib or control pre-treated tumor cells at a ratio of 1:8 tumor cells:T cells (*MMTV-PyMT*-S2WTP3-OVA) or 1:4 tumor cells:T cells (B16-OVA) in a final concentration of 10 μg/mL of the appropriate antibody with 2.5 ng/mL IL-7 (Peprotech), 50 ng/mL IL-15 (Peprotech), and 2 ng/mL IL-2 (Peprotech) for 48 hrs (*MMTV-PyMT*-S2WTP3-OVA) or 72 hrs (B16-OVA) at 37°C in the dark. At the experimental endpoint, cytokines in conditioned media were analyzed by ELISA, and CD8$^+$ T cell proliferation was determined by CFSE-dilution by flow cytometry.

Overexpression vectors and transfection

MMTV-PyMT-S2WTP3 cells were infected with lentiviral particles expressing the pHAGE-deltaOA-zsGreen plasmid as previously described[6], and infected cells were isolated by FACS.

MDA-MB-453 and BT474 cells were transient transfected with pBabepuro3-p16Flag (Addgene Cat # 24934) using Lipofectamine 3000 (Thermo Fisher) according to the manufacturer's instructions. 72 hours after transfection cells were selected in puromycin for 48 hours. p16 overexpression was confirmed by anti-FLAG western blots.

For overexpression of DNMT1, MDA-MB-453 cells were transfected with the pcDNA3/Myc-DNMT1 vector (Addgene Cat #36939) using Lipofectamine 3000 according to the manufacturer's instructions. Cells were treated with abemaciclib 72 hrs after transfection.

ELISAs

Cells were treated with DMSO or abemaciclib (500 nM) for 7 days. For the last 24 hours, culture media was replaced with serum free media. Following concentration of conditioned medium using Amicon Ultra centrifugal filters (Millipore), cytokines were analyzed according to the manufacturer's recommendations: human IFN gamma ELISA Ready-SET-Go! (Affymetrix eBioscience), human TNF alpha ELISA Ready-SET-Go! (Affymetrix eBioscience), Verikine human IFN alpha ELISA kit (PBL assay science), VeriKine-HS human IFN beta serum ELISA kit (PBL assay science), human IL-28B quantikine ELISA kit (R&D Systems), human IL-28A DuoSet ELISA (R&D Systems), and human IL-29 DuoSet ELISA (R&D Systems). Cytokine production by OT-I T cells in OVA/OT-I co-culture assays was measured by mouse IFN gamma ELISA Ready-SET-Go! (Affymetrix eBioscience) and mouse TNF-alpha Quantikine ELISA Kit (R&D Systems) according to the manufacturer's instructions. Anti-ANA and anti-dsDNA ELISAs (Alpha Diagnostic) were performed on plasma according to the manufacturer's instructions. Absorbance was measured on a Synergy Neo plate reader (BioTek) using Gen5 software.

Interferon neutralization experiments

Cell lines were treated with DMSO or abemaciclib (500nM) for 7 days. For the duration of drug treatment, neutralizing antibodies were applied including: IFN gamma (1 μg/mL, R&D Systems, MAB2851), IFN alpha (2.0–2.5 μg/mL, R&D Systems, 21100-1), IL-28a (0.5 μg/mL, R&D Systems, MAB1587), or IL-29 (1 μg/mL, R&D Systems, MAB15981-100). Successful neutralization was validated using recombinant human IFN gamma (Peprotech, 250pg/mL) and IFN alpha (Life Technologies, 250pg/mL). Recombinant proteins were administered 24 hours prior to protein collection.

Analysis of methylation of the *ERV3-1* 5′-LTR

Genomic DNA was extracted from cells and subjected to RNAse treatment before standard bisulfite conversion (MethylEdge Bisulfite Kit, Promega). Bisulfite DNA was subjected to PCR, and then a second nested PCR, to amplify the 5′;-LTR of *ERV3-1* using the method and primers as previously described[30] to amplify a DNA fragment of 644bp. The PCR product was enzymatically digested using the RsaI restriction enzyme (New England Biolabs). Due to a CG site in the native DNA within this amplicon, this digestion will cut methylated DNA amplicons into ~ 317 bp and ~327 bp fragments, leaving the non-methylated DNA uncut.

shRNA experiments

Two shRNA constructs to *RB1* (TRC ID# TRCN0000295892 and TRCN0000295842) and shLuciferase control were expressed in tumor cells as previously described[6]. Suppression efficiency was validated by RT-qPCR.

Doxorubicin-induced senescence

MDA-MB-453 and BT474 cells were treated with doxorubicin (Sigma Aldrich, 200nM) for a period of 24 hrs. The cells were then cultured in fresh media for 72 hours after treatment, and RNA was extracted for qPCR.

In vitro regulatory T cell differentiation

$CD4^+CD25^-$ T cells were isolated from spleens and lymph nodes of naïve FVB mice using the $CD4^+CD25^+$ Regulatory T cell kit (Miltenyl Biotec) with an autoMACs pro separator. Cells were cultured for 72 hours in T cell medium with CD3/CD28 Dynabeads (1:1 ratio of cells:beads, ThermoFisher), 100 U/mL rhIL-2 (Peprotech), +/− 25 ng/mL rhTGF-β (R&D Systems) with DMSO or abemaciclib (125–1000 nM). Differentiation status for each condition was determined by intracellular flow cytometry for FoxP3. Fold change in percent differentiation with the addition of rhTGF-β was calculated for each condition and normalized to the DMSO control.

T cell proliferation *in vitro*

$CD4^+CD25^-$ and $CD4^+CD25^+$ T cells were isolated from spleens and lymph nodes of naïve FVB mice using the CD4+ CD25+ Regulatory T cell kit (Miltenyl Biotec); $CD8^+$ T cells were isolated as described above. Isolated T cells were labeled with 5 μM CFSE (Biolegend) as described above. 1×10^5 cells were cultured in T cell medium with CD3/CD28 beads (1:1

ratio of cells to beads), 100 U/mL rhIL-2 and DMSO or abemaciclib (250 or 500 nM) for 72 hours at 37°C. CFSE dilution was analyzed at endpoint by flow cytometry.

Gene expression in isolated T cell populations

$CD8^+$, $CD4^+CD25^-$, and $CD4^+CD25^+$ T cells were isolated as described above from lymph nodes and spleens of naïve FVB mice treated with vehicle or 90 mg/kg abemaciclib for 12 days. Purity of isolated populations was confirmed by flow cytometry. mRNA was obtained using the NucleoSpin RNA XS kit (Macherey-Nagel) according to the manufacturer's instructions. RT-qPCR was performed as described above.

Patient data

Gene expression data (GEO GSE93204) were obtained from biopsy samples from the NeoPalAna clinical trial (NCT01723774)[9]. Expression data was utilized in the log2 normalized form. We used GSEA software (Broad Institute, MA) with the following settings for analysis: Number of permutations: 1000; Collapse dataset of gene symbols: true; Permutation type: gene set; Enrichment statistic: weighted; Metric for ranking genes: Signal2Noise; Gene list sorting mode: real; Gene list ordering mode: descending; Max size/exclude larger sets: 500; Min size/exclude smaller sets: 15. Analysis was performed using the "Hallmarks v6.0" GSEA signatures.

Statistical analyses

Statistical analyses were performed as described in the figure legend for each experiment. All statistical tests were two-sided, and non-parametric tests were used when variance was dissimilar between groups. All data are presented as mean ± SD unless otherwise noted in the legend. Differences were considered statistically significant at a p value ≤ 0.05. All data shown is representative two or more independent experiments, unless indicated otherwise.

Data availability

Transcriptomic data that support the findings of this study have been deposited in the Gene Expression Omnibus with primary accession code GSE99063. Source data for Western blots and tumor measurements are provided in Supplementary Fig. 1 and Supplementary Table 2. All other data is available upon reasonable request.

Extended Data

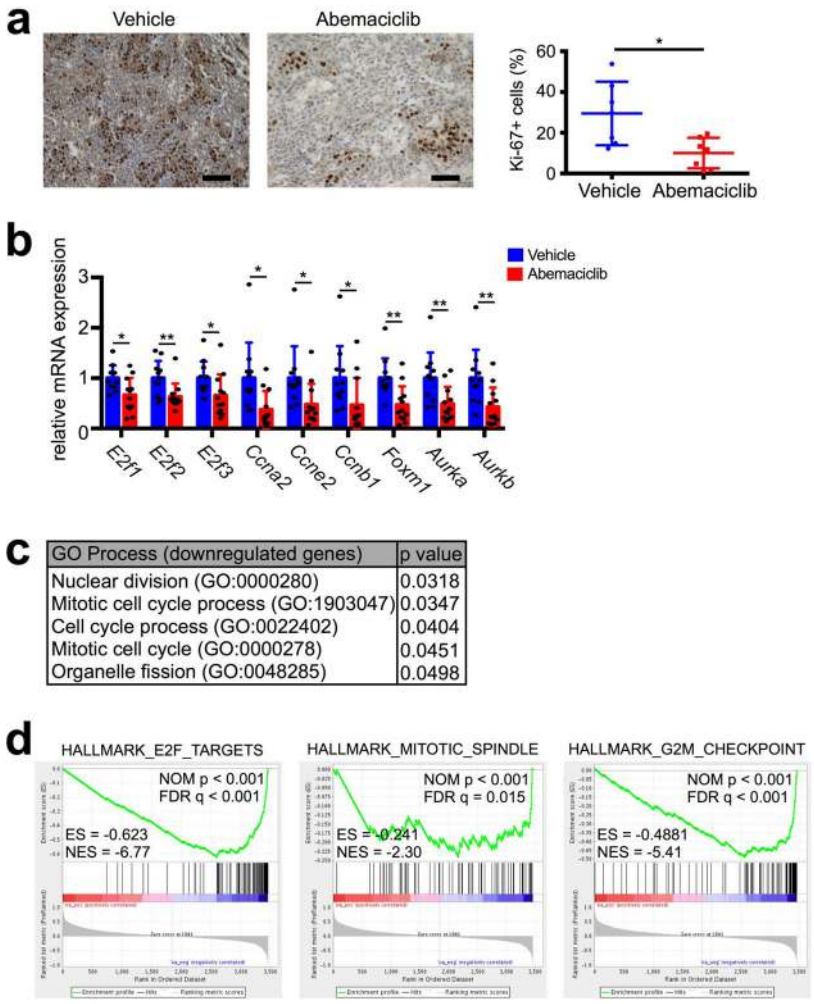

GO Process (downregulated genes)	p value
Nuclear division (GO:0000280)	0.0318
Mitotic cell cycle process (GO:1903047)	0.0347
Cell cycle process (GO:0022402)	0.0404
Mitotic cell cycle (GO:0000278)	0.0451
Organelle fission (GO:0048285)	0.0498

Extended Data Figure 1. Tumor cell proliferation and expression of cell cycle related genes after CDK4/6 inhibition

a, Immunohistochemistry for Ki-67 in *MMTV-rtTA/tetO-HER2* tumors treated for 12d with abemaciclib or vehicle; representative images (scale bar=100 μm) and quantification (n=7 tumors/group). **b**, Expression of E2F transcription factors, S phase genes, and G2/M genes in *MMTV-rtTA/tetO-HER2* tumors treated with abemaciclib for 12d compared to vehicle (vehicle, n=11; abemaciclib, n=12 tumors). **c–d**, Gene ontology terms with p<0.05 (c) or GSEA terms significantly downregulated (d) by abemaciclib compared to vehicle in *MMTV-rtTA/tetO-HER2* tumors (vehicle, n=11; abemaciclib, n=12 tumors). Unpaired two-tailed t-tests (a–b). Error bars, SD. *p<0.05, **p<0.01.

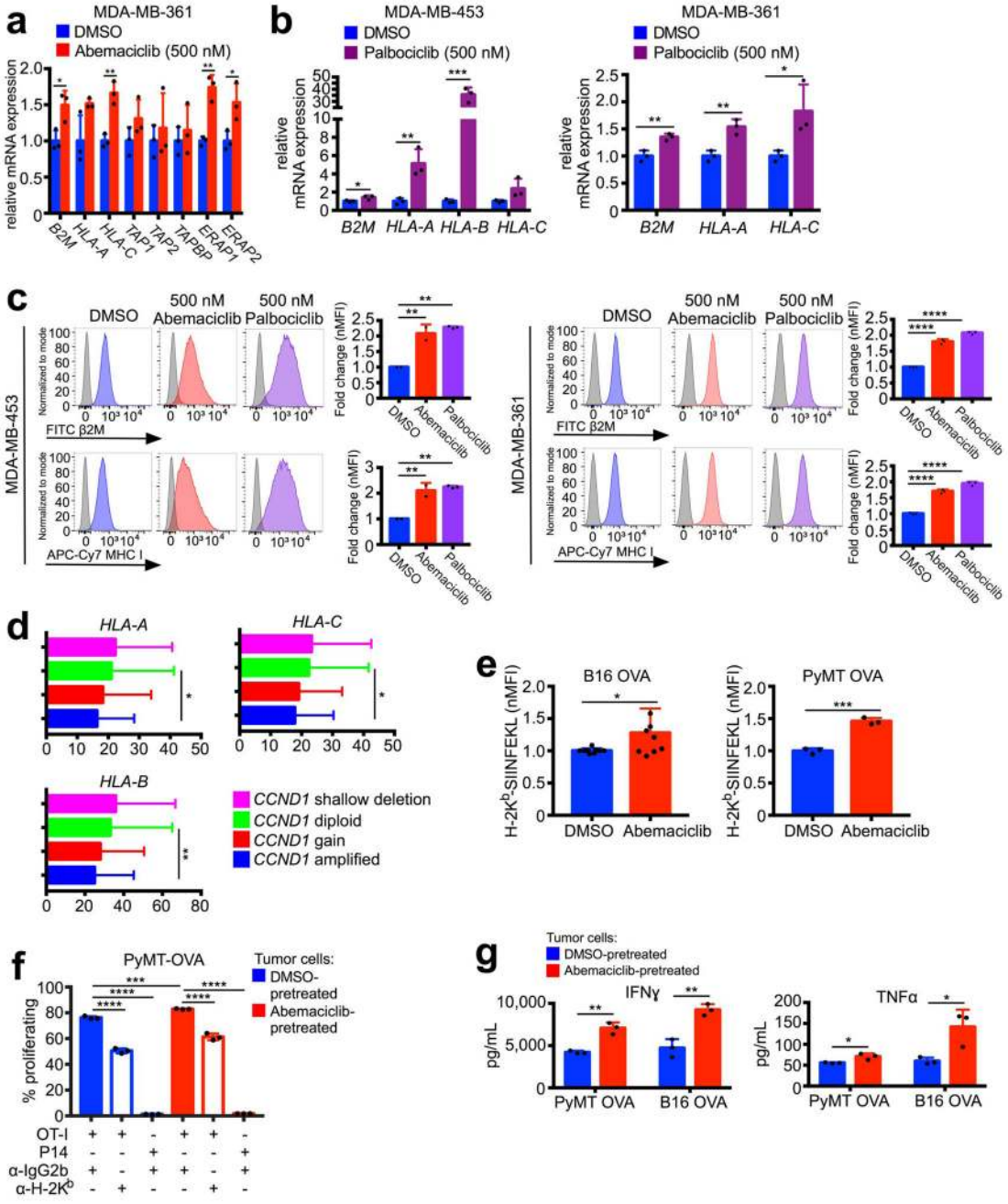

Extended Data Figure 2. CDK4/6 inhibition enhances antigen presentation

a, Antigen processing and presentation gene expression in MDA-MB-361 cells treated with 500 nM abemaciclib or DMSO (7d, n=3). **b**, Gene expression in cell lines treated with DMSO or palbociclib (7d, n=3). **c**, β2M/MHC-I flow cytometry in cell lines; grey, FMO control. (For MDA-MB-453, vehicle and abemaciclib, n=2; palbociclib, n=3. For MDA-MB-361, n=3) **d**, Gene expression in TCGA samples (*CCND1* shallow deletion, n=101; *CCND1* diploid, n=503; *CCND1* gain, n=203; *CCND1* amplified, n=153). **e**, H-2K^b SIINFEKL flow cytometry after 7d abemaciclib or DMSO (B16-OVA, n=9; *MMTV-PyMT-*

S2WTP3-OVA, n=3). **f**, CD8+ T cell proliferation in response to abemaciclib-pretreated tumor cells (n=3). **g**, IFNγ and TNFα production in tumor cell/OT-I assay by ELISA (n=3). One-way ANOVA adjusted for multiple comparisons (c–d,f), unpaired two-tailed t-tests (a–b,e,g). Error bars, SD. *p<0.05, **p<0.01, ***p<0.001, ****p<0.0001.

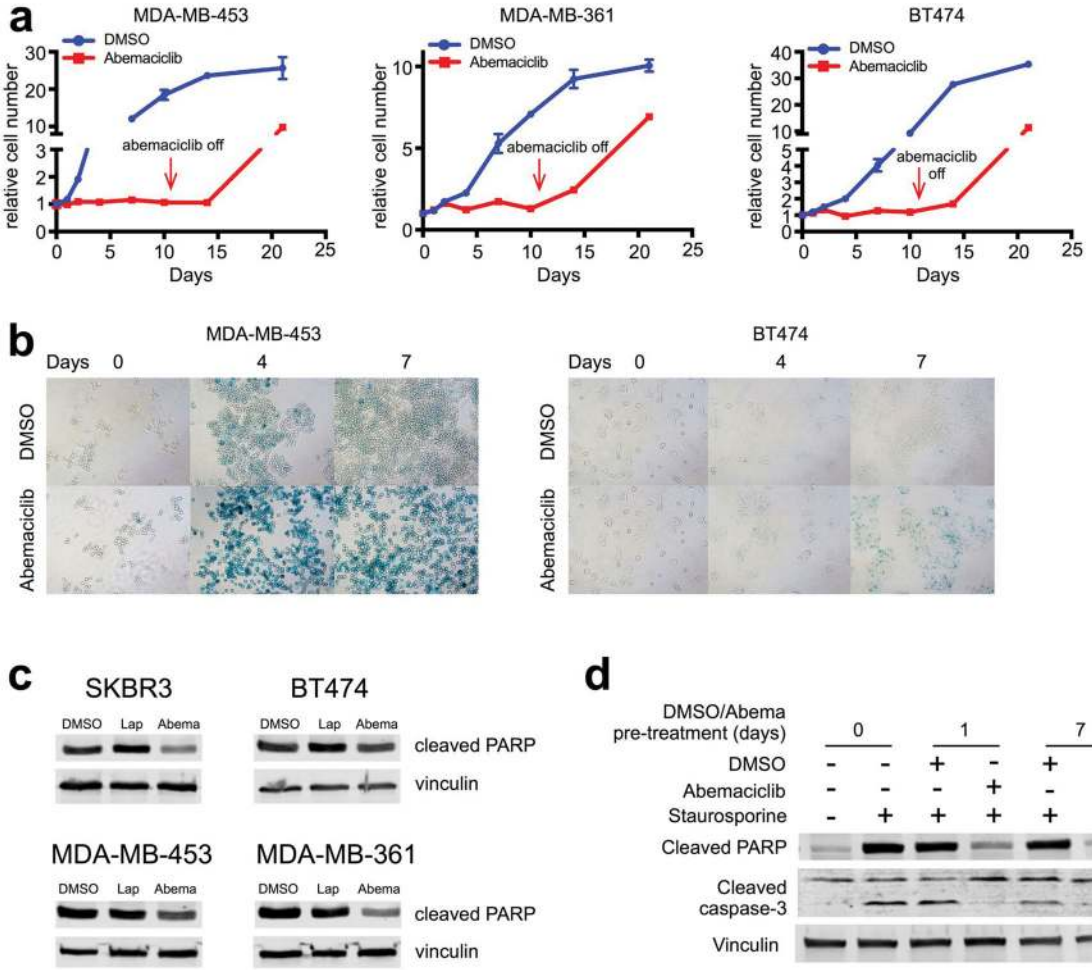

Extended Data Figure 3. Effects of CDK4/6 inhibition on breast cancer cell proliferation and apoptosis *in vitro*

a, Relative numbers of breast cancer cells cultured in 250 nM (MDA-MB-453) or 500 nM (MDA-MB-361, BT474) abemaciclib or DMSO for 11d, followed by drug withdrawal (arrow). **b**, Representative SA-β-galactosidase staining of MDA-MB-453 cells (left) and BT474 cells (right) treated with DMSO or abemaciclib (MDA-MB-453, 250 nM; BT474, 500 nM) for 0, 4, and 7 days. **c**, Western blot of SKBR3, BT474, MDA-MB-453, and MDA-MB-361 cells treated with DMSO, lapatinib, or abemaciclib for 48h. **d**, Western blot of MDA-MB-453 cells pretreated with DMSO or abemaciclib (500 nM) for 0, 1, or 7 days prior to exposure to staurosporine (500 nM) for 4h. For western blot source images, see Supplementary Figure 1.

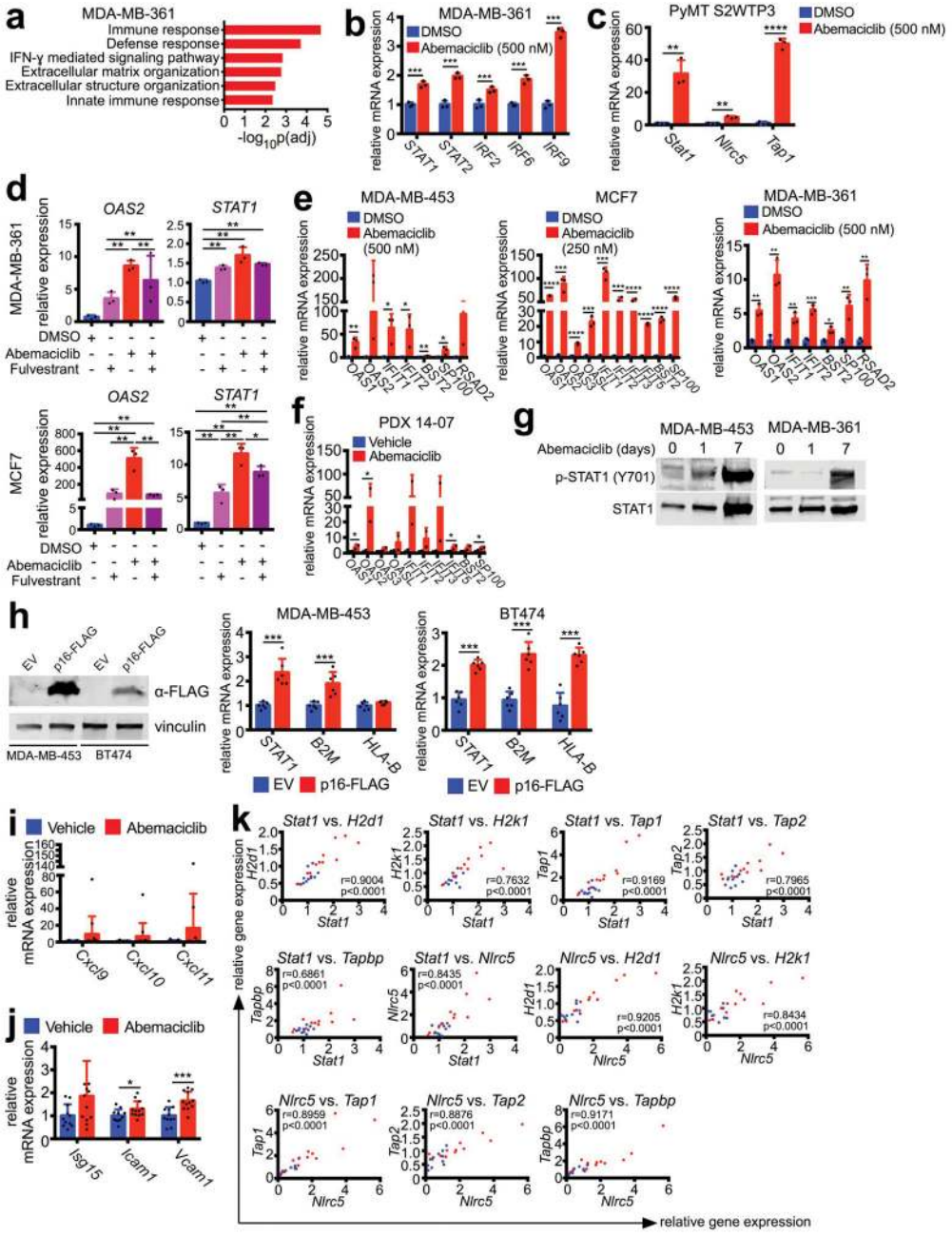

Extended Data Figure 4. CDK4/6 inhibition increases interferon signaling

a–b, Top ranked GO terms (a) and expression of interferon-responsive transcription factors (b) in MDA-MB-361 cells treated with 500 nM abemaciclib or DMSO (7d, n=3). **c**, Expression of interferon sensitive genes (ISGs) in *MMTV-PyMT*-S2WTP3 cells treated with DMSO or abemaciclib (500 nM, 7d) (n=3). **d**, Expression of ISGs in MDA-MB-361 and MCF7 cells treated with abemaciclib (100 nM), fulvestrant (100 nM), or the combination for 7d (n=3). **e**, Expression of ISGs in MDA-MB-453, MCF7, and MDA-MB-231 cells treated with abemaciclib or DMSO (7d, n=3). **f**, Expression of ISGs in PDX 14-07 tumors treated with abemaciclib or vehicle (21–28d, vehicle, n=4; abemaciclib, n=2 tumors/group). **g**,

phospho- and total STAT1 in cells treated with 500 nM abemaciclib as indicated. **h**, Confirmation of p16-FLAG overexpression in MDA-MB-453 and BT474 cells (left) and gene expression in these cell lines by qPCR (right) (n=6). **i–j**, Gene expression changes in *MMTV-rtTA/tetO-HER2* tumors from mice treated with vehicle or abemaciclib for 12d (vehicle, n=11; abemaciclib, n=12 tumors/group). Relative expression of interferon-responsive T cell chemoattractants (i); relative expression of ISGs (j). **k**, Correlation of expression of Stat1 and Nlrc5 with genes involved in antigen processing and presentation in *MMTV-rtTA/tetO-HER2* tumors. Blue dots, vehicle-treated tumors; red dots, abemaciclib-treated tumors. (r is Pearson product-moment correlation coefficient). Unpaired two-tailed t-tests (b,d–f,h–j) adjusted for multiple comparisons (c). Error bars, SD. *p<0.05, **p<0.01, ***p<0.001, ****p<0.0001. For western blot source images, see Supplementary Figure 1.

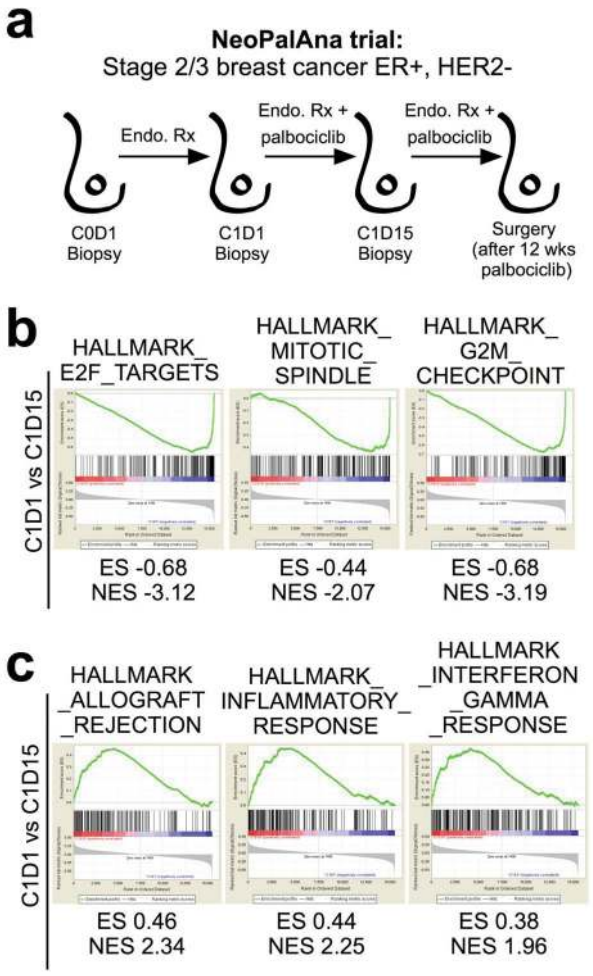

Extended Data Figure 5. CDK4/6 inhibitors enhance expression of immune-related signatures in breast cancer patients

a–c, NeoPalAna schema (a) Endo. Rx denotes endocrine therapy for breast cancer. Down-regulated GSEA signatures after 2 wks palbociclib treatment (b); Nom p<0.001, FDR q<0.001. Up-regulated GSEA signatures after 2 wks palbociclib treatment (c); Nom p<0.001, FDR q<0.001 (C1D1, n=34; C1D15, n=29; Surgery, n=23).

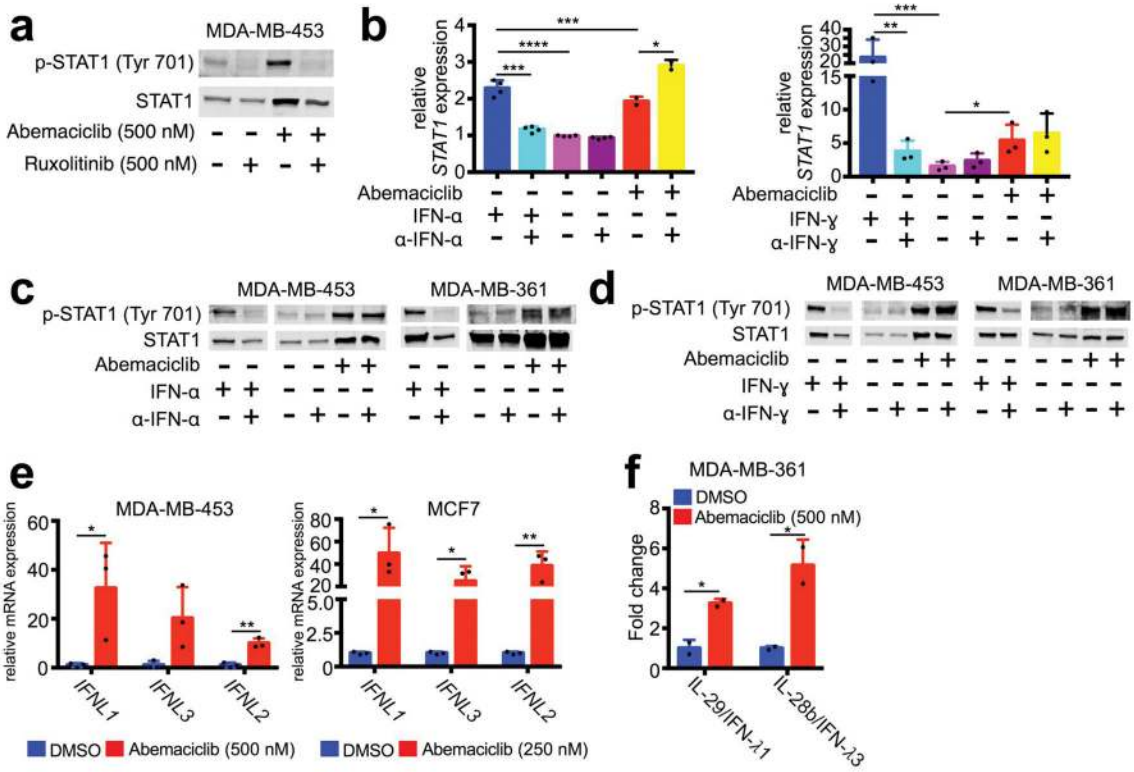

Extended Data Figure 6. CDK4/6 inhibition mediates Type III interferon production

a, Phospho- and total STAT1 in MDA-MB-453 cells treated with abemaciclib +/− ruxolitinib for 7d. **b**, Effect of neutralization of IFN-α or IFN-γ on STAT1 mRNA expression (n=2–4). **c**–**d**, Impact of neutralization of IFN-α (c) and IFN-γ (d) on phospho-STAT1 and total STAT1 protein in indicated cell lines. **e**, Expression of type III interferon genes in indicated cell lines treated with abemaciclib for 7d compared to DMSO (n=3). **f**, Type III interferon production measured by ELISA (7d, n=2). Unpaired two-tailed t-tests (e–f) adjusted for multiple comparisons (b). Error bars, SD. *p<0.05, **p<0.01, ***p<0.001, ****p<0.0001. For western blot source images, see Supplementary Figure 1.

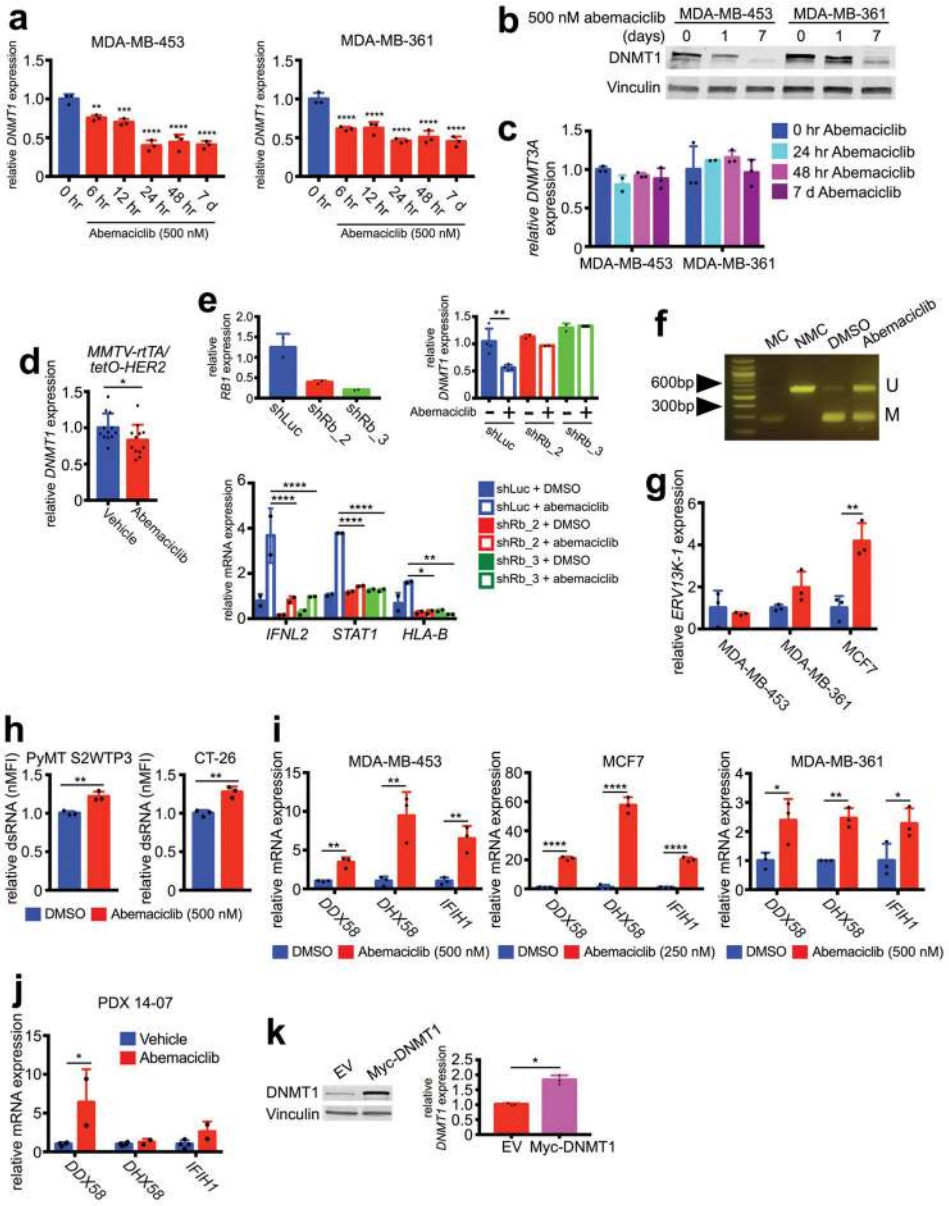

Extended Data Figure 7. DNMT1 suppression mediates dsRNA response

a, *DNMT1* expression after treatment with abemaciclib (n=3). **b**, DNMT1 protein expression after treatment with abemaciclib. **c**, *DNMT3A* expression after treatment with abemaciclib (500 nM) for 7d (n=3, except abemaciclib 24 hrs, n=2). **d**, *DNMT1* expression after abemaciclib or control in *MMTV-rtTA/tetO-HER2* tumors, p=0.05, (12d, vehicle, n=11; abemaciclib, n=12 tumors/group). **e**, *RB1* knockdown in MDA-MB-453 cells and its effect on indicated gene expression after 7d abemaciclib (500 nM) (two biological replicates each associated with three technical replicates). **f**, *ERV3-1* methylation. **g**, ERV expression after abemaciclib or DMSO (7d, n=3). **h**, Relative dsRNA expression after 7d of abemaciclib compared to DMSO (n=3). **i–j**, Cytosolic pattern recognition receptors in cells (i) (7d, n=3) or PDX tumors (j) (21–28d, vehicle, n=4; abemaciclib, n=2 tumors/group). **k**, Western blot

of overexpression of DNMT1 in MDA-MB-453 cells and quantification of mRNA expression (n=3). Unpaired two-tailed t-tests (d–e,g–k) adjusted for multiple comparisons (a). Error bars, SD. *p ≤0.05, **p<0.01, ***p<0.001, ****p<0.0001. For western blot source images, see Supplementary Figure 1.

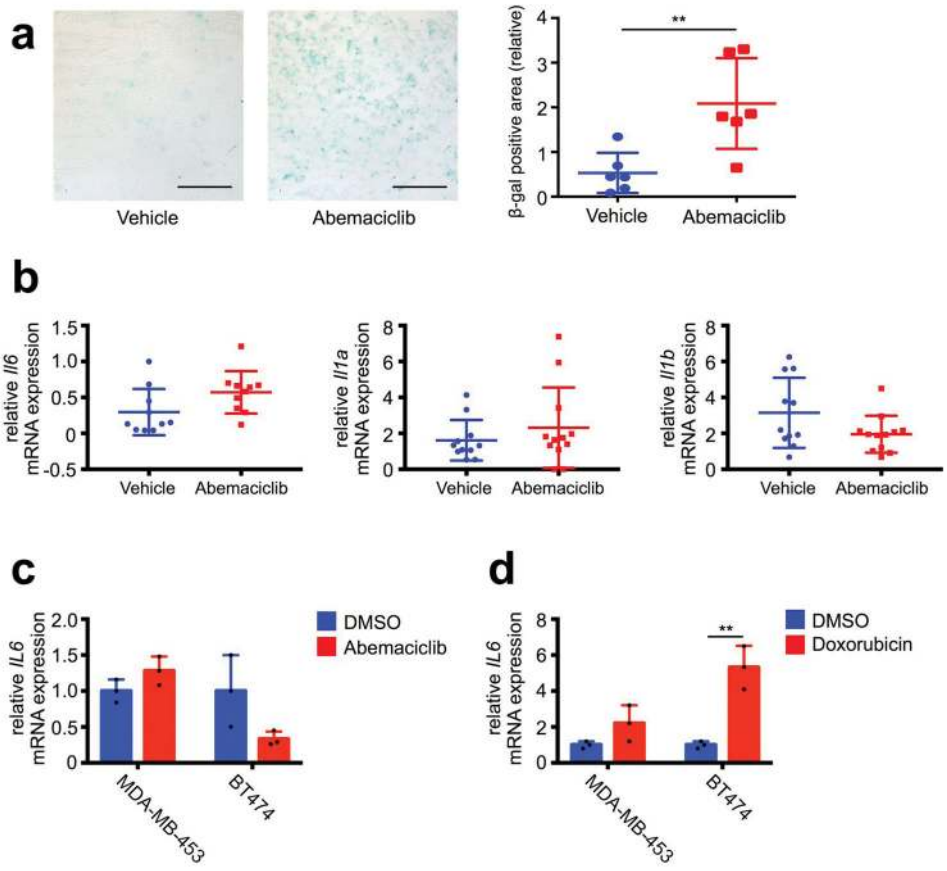

Extended Data Figure 8. Abemaciclib induces a 'senescence-like' phenotype without evidence of SASP

a, Representative SA-β-galactosidase staining (left) of *MMTV-rtTA/tetO-HER2* tumors treated with vehicle or abemaciclib for 12d (scale bar=500 μm). Quantification of relative SA-β-galactosidase positive area (right, n=6 tumors/group). **b**, mRNA expression of SASP factors in *MMTV-rtTA/tetO-HER2* tumors treated as in Fig. 1a. *Il6* expression determined by qPCR (n=10 tumors/group); *Il1a* and *Il1b* by transcriptome analysis (vehicle, n=11; abemaciclib, n=12 tumors/group). **c**, MDA-MB-453 and BT474 cells treated with DMSO or abemaciclib (500 nM) for 7d, and expression determined by qPCR. **d**, mRNA expression of *IL6* upon doxorubicin-induced senescence (n=3). MDA-MB-453 and BT474 cells were treated with doxorubicin (200 nM) for 24h, and mRNA extracted 3d later for qPCR. Unpaired two-tailed t tests (a,d). Error bars, SD. **p<0.01.

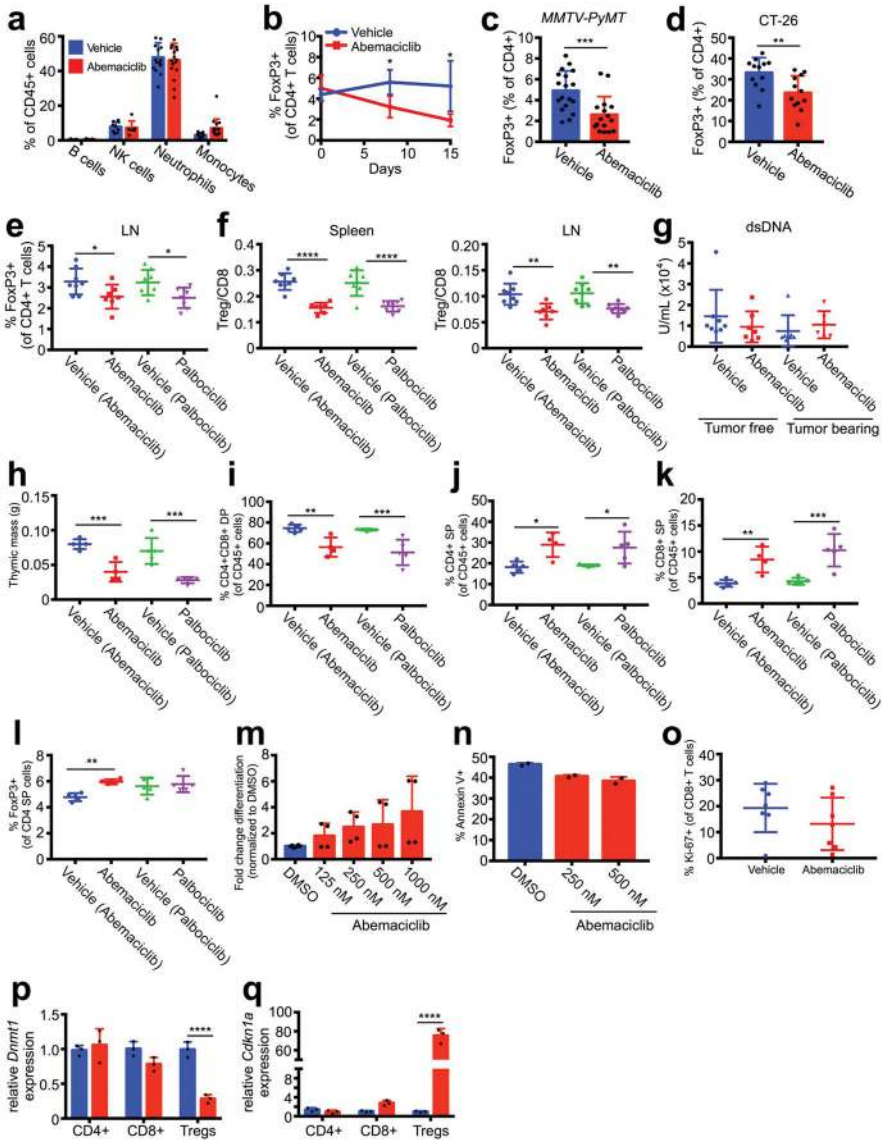

Extended Data Figure 9. Impact of CDK4/6 inhibition on immune cell populations and Treg biology

a, Flow cytometric analysis of immune cell populations in *MMTV-rtTA/tetO-HER2* tumors treated with vehicle or abemaciclib for 12d (vehicle, n=15; abemaciclib, n=17 tumors/group). **b**, Peripheral blood Tregs in *MMTV-rtTA/tetO-HER2* mice (12d, n=4 mice/group). **c–d**, Tregs ($CD4^+$ $FoxP3^+$) quantified by flow cytometry of *MMTV-PyMT* tumors (c, vehicle, n=18; abemaciclib, n=16 tumors/group) and CT-26 tumors (d, n=12 tumors/group) treated as indicated for 12d. **e**, Tregs in lymph nodes of tumor-free mice (12d, one-way ANOVA corrected for multiple comparisons, vehicles and palbociclib, n=8; abemaciclib, n=7 mice/group). **f**, Treg:CD8 ratio in the spleens and lymph nodes (LN) of tumor-free FVB mice (12d, vehicles and palbociclib, n=8; abemaciclib, n=7 mice/group). **g**, Plasma autoantibodies in tumor-free and tumor-bearing mice treated with vehicle or abemaciclib for 12d (tumor-free vehicle, n=8; tumor-free abemaciclib, n=7; tumor-bearing vehicle, n=7;

tumor-bearing abemaciclib, n=6 mice/group). **h–l**, Tumor-free FVB mice treated with abemaciclib or vehicle for 12d. Thymic mass (h). Thymic cell populations were quantified by flow cytometry. $CD4^+CD8^+$ double positive (DP) thymocytes (i); $CD4^+$ single positive (SP) thymocytes (j); $CD8^+$ SP thymocytes (k); $CD4^+FoxP3^+$ regulatory T cells (l). (vehicles and palbociclib, n=5; abemaciclib, n=4 mice/group). **m**, Effect of abemaciclib or DMSO on *ex vivo* differentiation of $CD4^+CD25^-$ T cells into Tregs in the presence of TGF-β for 72hr (n=4). **n**, Effect of DMSO or abemaciclib treatment for 72hr on Treg apoptosis measured by Annexin V staining (n=2). **o**, Quantification of immunofluorescent staining of *MMTV-rtTA/tetO-HER2* tumors (n=7 tumors/group). **p–q**, *Dnmt1* (p) and *Cdkn1a* (q) in T cells from tumor-free mice (12d, two-way ANOVA corrected for multiple comparisons, n=7 mice/group [pooled]). Unpaired two-tailed t-tests (b–d), one-way ANOVA corrected for multiple comparisons (e–f,h–l). Error bars, SD. *p<0.05, **p<0.01, ***p<0.001, ****p<0.0001

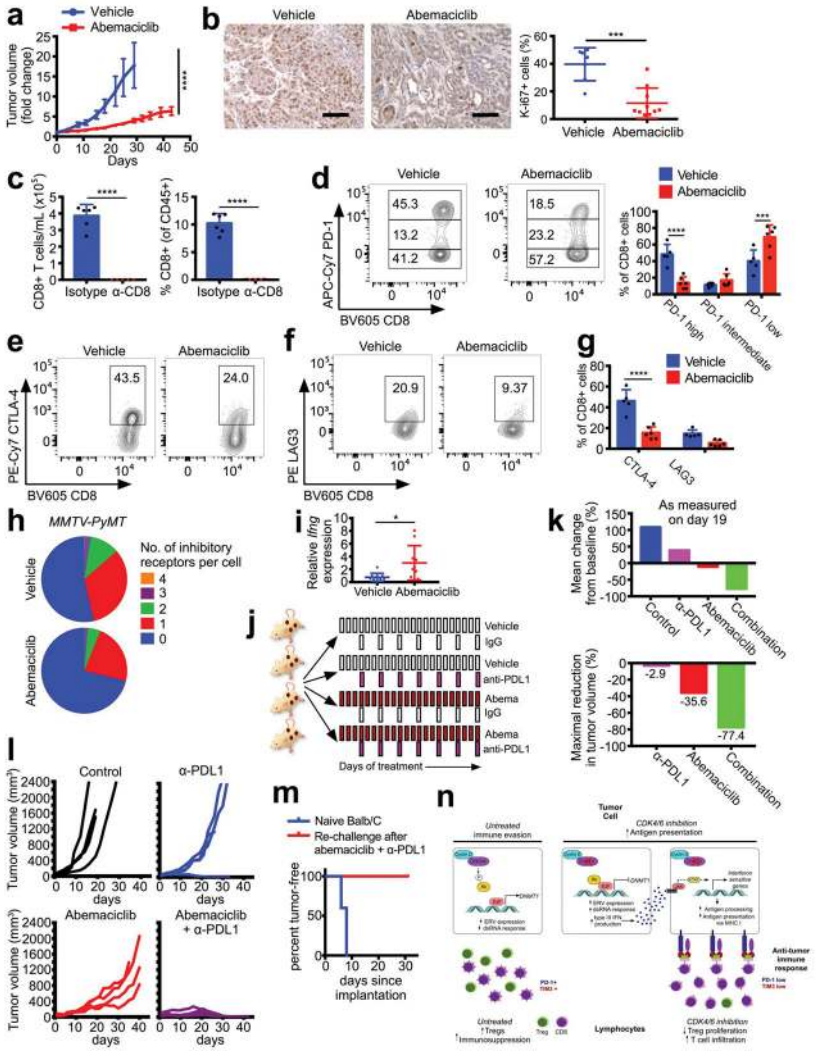

Extended Data Figure 10. Role of adaptive immunity in response to abemaciclib and combination with immunotherapy

a, Relative change in volume of *MMTV-rtTA/tetO-HER2* tumors implanted into *Foxn1*^{nu} mice and then treated with vehicle (n=11 tumors) or abemaciclib (n=9 tumors) (one way ANOVA). **b**, Immunohistochemistry of tumors in (a) for Ki-67. Representative images (left), and quantification of percent of Ki-67^{+} cells (right) (vehicle, n=7; abemaciclib, n=10/group, scale bar=100 μm). **c**, Flow cytometric analysis of absolute number (left) and percentage (right) of CD8^{+} T cells in peripheral blood after administration of anti-CD8 or isotype control antibodies (isotype, n=6; anti-CD8, n=4 mice/group). **d–g**, Expression of inhibitory co-receptors on intratumoral CD8^{+} T cells in *MMTV-rtTA/tetO-HER2* tumors after 6d of treatment with abemaciclib (n=6 tumors) or vehicle (n=5 tumors). PD-1 cell-surface expression (d); representative flow cytometry plots (left), quantification (right). Representative flow cytometry plots for CTLA-4 (e) and LAG3 (f). **g,** Quantification of (e) and (f). **h**, Quantification of number of inhibitory receptors per cell on intratumoral CD8+ T cells in *MMTV-PyMT* tumors after treating mice with abemaciclib or vehicle (12d, n=18 tumors/group). **i**, *Ifng* in *MMTV-rtTA/tetO-HER2* tumors (12d, Mann-Whitney test, n=10 tumors/group). **j**, Experimental schema for Fig. 4j. **k**, Quantification of mean change in tumor volume at d19 (top) and maximal reduction in tumor volume (bottom) of curves in Fig. 4j. **l**, Spider plots of CT-26 tumor growth with indicated treatments (n=4/group, one experiment). **m**, Kaplan-Meier curves of incidence of CT-26 tumor formation after rechallenge. **n**, Schematic. Unpaired two-tailed t-tests (b–c), two-way ANOVA corrected for multiple comparisons (d,g). Error bars, SD; except (a), SEM. *p<0.05, ***p<0.001, ****p<0.0001. For source data, see Supplementary Table 2.

Supplementary Material

Refer to Web version on PubMed Central for supplementary material.

Acknowledgments

This work was supported by a Career Development Award from the DF/HCC SPORE in Breast Cancer (NIH 2015 P50 CA, to S.G.), Landry Cancer Biology Research Fellowship (to M.J.D.), DOD Era of Hope award (W81XWH-14-1-0191 to S.S.M), NIH (NCI) RO1 CA166284 (to S.S.M), a Presidential Early Career Award for Scientists and Engineers (to S.S.M), the Breast Cancer Research Foundation (to J.J.Z), the DF/HCC SPORE in Breast Cancer (P50 CA168504, to I.E.K., E.P.W., T.M.R. and J.J.Z), and NIH awards CA187918-02 (to T.M.R. and J.J.Z), CA210057-01 (to J.J.Z), and CA172461-04 (to J.J.Z). We thank Tyler Laszewski, Anna Molineaux, Jamie Almeida, the Nikon Imaging Center at Harvard Medical School, and Boston Children's Hospital Heme/Onc-HSCI Flow Cytometry facility for experimental assistance. We thank providers of reagents: pHAGE-deltaOVA-zsGreen plasmid (Rong En Tay, Kai Wucherpfennig), *LCMV-P14* transgenic mice (Adam Cartwright, Kai Wucherpfennig), CT-26 cell line (Stephen Elledge), *MMTV-PyMT*-S2WTP3 cell line (Andreas Moller). We thank Sheila Stewart for advice.

References

1. Yu Q, et al. Requirement for CDK4 kinase function in breast cancer. Cancer Cell. 2006; 9:23–32. DOI: 10.1016/j.ccr.2005.12.012 [PubMed: 16413469]
2. Choi YJ, et al. The requirement for cyclin D function in tumor maintenance. Cancer Cell. 2012; 22:438–451. DOI: 10.1016/j.ccr.2012.09.015 [PubMed: 23079655]
3. Patnaik A, et al. Efficacy and Safety of Abemaciclib, an Inhibitor of CDK4 and CDK6, for Patients with Breast Cancer, Non-Small Cell Lung Cancer, and Other Solid Tumors. Cancer Discov. 2016; 6:740–753. DOI: 10.1158/2159-8290.CD-16-0095 [PubMed: 27217383]
4. Finn RS, et al. Palbociclib and Letrozole in Advanced Breast Cancer. N Engl J Med. 2016; 375:1925–1936. DOI: 10.1056/NEJMoa1607303 [PubMed: 27959613]

5. Sherr CJ, Roberts JM. CDK inhibitors: positive and negative regulators of G1-phase progression. Genes Dev. 1999; 13:1501–1512. [PubMed: 10385618]
6. Goel S, et al. Overcoming Therapeutic Resistance in HER2-Positive Breast Cancers with CDK4/6 Inhibitors. Cancer Cell. 2016; 29:255–269. DOI: 10.1016/j.ccell.2016.02.006 [PubMed: 26977878]
7. Cerami E, et al. The cBio cancer genomics portal: an open platform for exploring multidimensional cancer genomics data. Cancer Discov. 2012; 2:401–404. DOI: 10.1158/2159-8290.CD-12-0095 [PubMed: 22588877]
8. Campisi J, di Fagagna FA. Cellular senescence: when bad things happen to good cells. Nature Reviews Molecular Cell Biology. 2007; 8:729–740. [PubMed: 17667954]
9. Ma CX, et al. NeoPalAna: Neoadjuvant palbociclib, a cyclin-dependent kinase 4/6 inhibitor, and anastrozole for clinical stage 2 or 3 estrogen receptor positive breast cancer. Clin Cancer Res. 2017
10. Roulois D, et al. DNA-Demethylating Agents Target Colorectal Cancer Cells by Inducing Viral Mimicry by Endogenous Transcripts. Cell. 2015; 162:961–973. [PubMed: 26317465]
11. Kimura H, Nakamura T, Ogawa T, Tanaka S, Shiota K. Transcription of mouse DNA methyltransferase 1 (Dnmt1) is regulated by both E2F-Rb-HDAC-dependent and -independent pathways. Nucleic Acids Res. 2003; 31:3101–3113. [PubMed: 12799438]
12. Chiappinelli KB, et al. Inhibiting DNA Methylation Causes an Interferon Response in Cancer via dsRNA Including Endogenous Retroviruses. Cell. 2015; 162:974–986. [PubMed: 26317466]
13. Coppe JP, Desprez PV, Krtolica A, Campisi J. The Senescence-Associated Secretory Phenotype: The Dark Side of Tumor Suppression. Annu Rev Pathol. 2010; 5:99–118. [PubMed: 20078217]
14. Malumbres M, et al. Mammalian Cells Cycle without the D-Type Cyclin-Dependent Kinases Cdk4 and Cdk6. Cell. 2004; 118:493–504. [PubMed: 15315761]
15. Obata Y, et al. The epigenetic regulator Uhrf1 facilitates the proliferation and maturation of colonic regulatory T cells. Nat Immunol. 2014; 15:571–579. DOI: 10.1038/ni.2886 [PubMed: 24777532]
16. Bauer CA, et al. Dynamic Treg interactions with intratumoral APCs promote local CTL dysfunction. J Clin Invest. 2014; 124:2425–2440. DOI: 10.1172/JCI66375 [PubMed: 24812664]
17. Sakuishi K, et al. Targeting Tim-3 and PD-1 pathways to reverse T cell exhaustion and restore anti-tumor immunity. J Exp Med. 2010; 207:2187–2194. DOI: 10.1084/jem.20100643 [PubMed: 20819927]
18. Finn RS, et al. PD 0332991, a selective cyclin D kinase 4/6 inhibitor, preferentially inhibits proliferation of luminal estrogen receptor-positive human breast cancer cell lines in vitro. Breast Cancer Res. 2009; 11:R77. [PubMed: 19874578]
19. Heng TS, Painter MW. Immunological Genome Project, C. The Immunological Genome Project: networks of gene expression in immune cells. Nat Immunol. 2008; 9:1091–1094. DOI: 10.1038/ni1008-1091 [PubMed: 18800157]
20. Bates GJ, et al. Quantification of regulatory T cells enables the identification of high-risk breast cancer patients and those at risk of late relapse. J Clin Oncol. 2006; 24:5373–5380. DOI: 10.1200/JCO.2006.05.9584 [PubMed: 17135638]
21. McAllister SS, et al. Systemic endocrine instigation of indolent tumor growth requires osteopontin. Cell. 2008; 133:994–1005. DOI: 10.1016/j.cell.2008.04.045 [PubMed: 18555776]
22. Wong CS, et al. Vascular normalization by loss of Siah2 results in increased chemotherapeutic efficacy. Cancer Res. 2012; 72:1694–1704. DOI: 10.1158/0008-5472.CAN-11-3310 [PubMed: 22354750]
23. Bellone M, et al. Relevance of the tumor antigen in the validation of three vaccination strategies for melanoma. J Immunol. 2000; 165:2651–2656. [PubMed: 10946294]
24. Ni J, et al. Combination inhibition of PI3K and mTORC1 yields durable remissions in mice bearing orthotopic patient-derived xenografts of HER2-positive breast cancer brain metastases. Nat Med. 2016; 22:723–726. DOI: 10.1038/nm.4120 [PubMed: 27270588]
25. Wang Y, et al. CDK7-dependent transcriptional addiction in triple-negative breast cancer. Cell. 2015; 163:174–186. DOI: 10.1016/j.cell.2015.08.063 [PubMed: 26406377]
26. Love MI, Huber W, Anders S. Moderated estimation of fold change and dispersion for RNA-seq data with DESeq2. Genome Biol. 2014; 15:550. [PubMed: 25516281]

27. Subramanian A, et al. Gene set enrichment analysis: a knowledge-based approach for interpreting genome-wide expression profiles. Proc Natl Acad Sci U S A. 2005; 102:15545–15550. DOI: 10.1073/pnas.0506580102 [PubMed: 16199517]

28. Mootha VK, et al. PGC-1alpha-responsive genes involved in oxidative phosphorylation are coordinately downregulated in human diabetes. Nat Genet. 2003; 34:267–273. DOI: 10.1038/ng1180 [PubMed: 12808457]

29. Gao J, et al. Integrative analysis of complex cancer genomics and clinical profiles using the cBioPortal. Sci Signal. 2013; 6:pl1. [PubMed: 23550210]

30. Gimenez J, et al. Comparative methylation of ERVWE1/syncytin-1 and other human endogenous retrovirus LTRs in placenta tissues. DNA Res. 2009; 16:195–211. DOI: 10.1093/dnares/dsp011 [PubMed: 19561344]

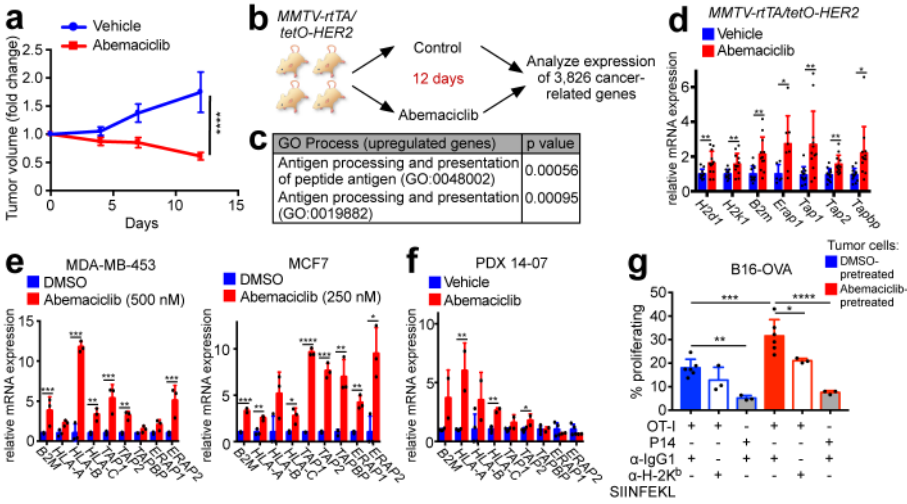

Figure 1. CDK4/6 inhibitors induce tumor regression and increase antigen presentation

a, Impact of abemaciclib treatment on *MMTV-rtTA/tetO-HER2* tumor volume (two-way ANOVA, vehicle, n=17; abemaciclib, n=22 tumors). **b–d**, *In vivo* experimental schema depicted in (b) (vehicle, n=11; abemaciclib, n=12 tumors). Gene ontology terms with p<0.05 (c) and expression of antigen presentation genes (d) are shown. **e–f**, Antigen presentation gene expression in cells (e) (7d, n=3) and PDX tumors (f) (21–28d, vehicle, n=4; abemaciclib, n=2 tumors) after abemaciclib treatment. **g**, $CD8^+$ T cell proliferation in response to abemaciclib-pretreated B16-OVA cells (OT-I + anti-IgG1, n=6; other conditions, n=3; one-way ANOVA adjusted for multiple comparisons) Unpaired two-tailed t-tests (d–f). Error bars SD; except (a), SEM. *p<0.05, **p<0.01, ***p<0.001, ****p<0.0001. For source data, see Supplementary Table 2.

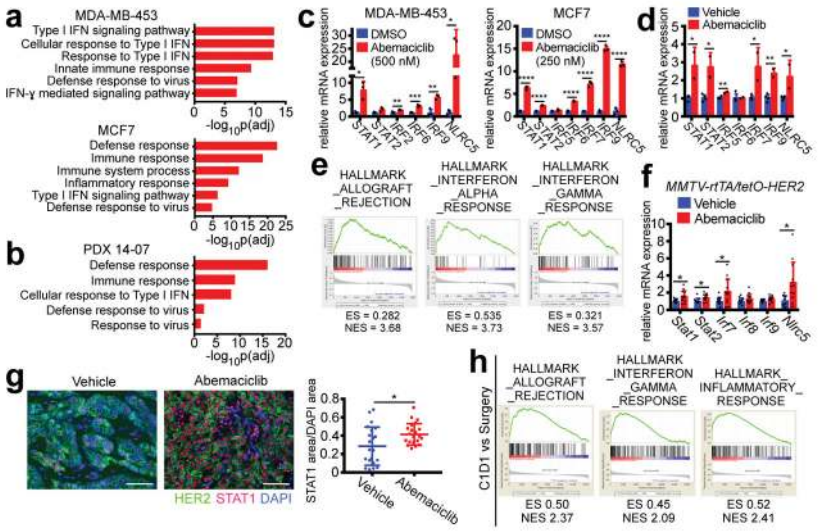

Figure 2. CDK4/6 inhibition stimulates interferon signaling

a–**b**, Top ranked GO terms in abemaciclib-treated tumor cells (a) (7d, n=3) or PDX tumors (b) (21–28d, vehicle, n=4; abemaciclib, n=2 tumors). **c–d,** Interferon-responsive gene expression from samples in (a) and (b). **e–f,** Upregulated GO terms (e) and expression of interferon-responsive transcription factors (f) in abemaciclib-treated *MMTV-rtTA/tetO-HER2* tumors (12d, vehicle, n=11; abemaciclib, n=12 tumors). **g**, *MMTV-rtTA/tetO-HER2* tumor STAT1 staining (12d, scale bar=100 μm, n=21). **h,** Upregulated GSEA signatures after 12wk of palbociclib in NeoAnaPal trial. (C1D1, n=34; surgery, n=23). Unpaired two-tailed tests (c, d, f); Mann-Whitney test (h); Error bars, SD. *p<0.05, **p<0.01, ***p<0.001, ****p<0.0001. For all GSEA, nom p<0.001, FDR q<0.001.

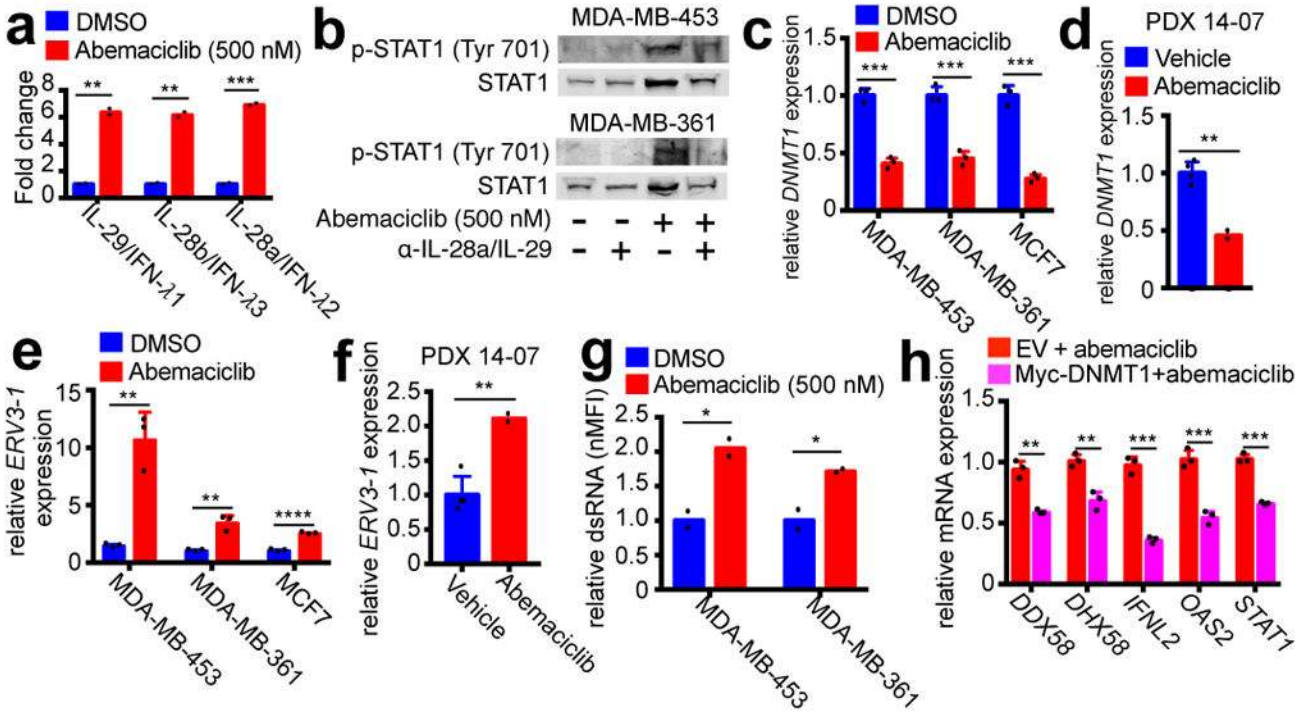

Figure 3. CDK4/6 inhibitors suppress DNMT1, inducing viral mimicry

a, Tumor cell type III interferon secretion measured by ELISA (7d)**. b**, Impact of Type III IFN neutralization on phospho- and total STAT1 protein (7d). **c–d**, *DNMT1* expression after abemaciclib or control in cells (b) (7d, n=3) or PDX tumors (d) (21–28d, vehicle, n=4; abemaciclib, n=2 tumors). **e–f**, *ERV3-1* expression in samples from (c) and (d). **g**, dsRNA levels in abemaciclib-treated tumor cells (7d, n=2). **h**, Effect of *DNMT1* overexpression on gene expression in MDA-MB-453 cells after 7d abemaciclib (50nM) (n=3). Abemaciclib at 500nM *in vitro*, unless noted, except MCF-7, 250nM. Unpaired two-tailed t-tests (a, c–h). Error bars, SD. *p<0.05, **p<0.01, ***p<0.001, ****p<0.0001. For western blot source images, see Supplementary Figure 1.

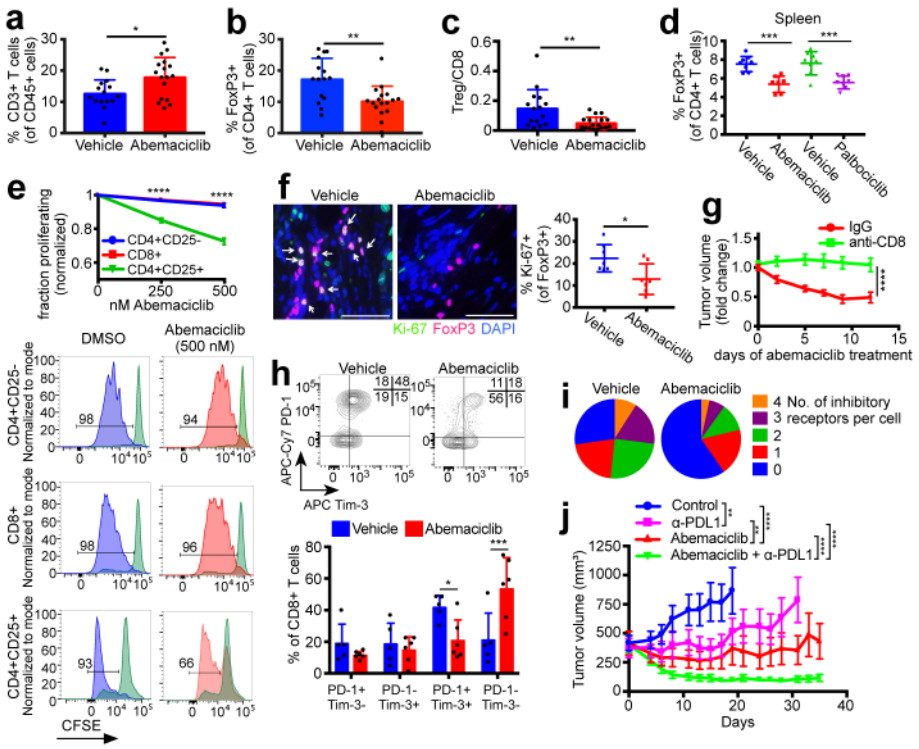

Figure 4. CDK4/6 inhibition modulates the immune milieu

a–c, Intratumoral T cells (a), Tregs (b), and Treg:CD8 ratios (c) in *MMTV-rtTA/tetO-HER2* tumors (12d treatment, vehicle, n=15; abemaciclib, n=17 tumors). **d,** Tregs in spleens of tumor-free mice (12d, vehicle and palbociclib, n=8; abemaciclib, n=7 mice). **e**, T cell proliferation *in vitro*. **f**, Ki-67/FoxP3 staining of *MMTV-rtTA/tetO-HER2* tumors (12d, scale bar=50 μm, n=7). **g**, *MMTV-rtTA/tetO-HER2* tumor volume after treatment with abemaciclib +–/ anti-CD8 neutralizing antibody (n=17 tumors). **h**, Inhibitory co-receptors on *MMTV-rtTA/tetO-HER2* intratumoral $CD8^+$ T cells (6d, vehicle, n=5; abemaciclib, n=6 tumors). **i,** Number of inhibitory receptors per cell on $CD8^+$ T cells from (h). **j**, *MMTV-rtTA/tetO-HER2* tumor volume after treatment with abemaciclib $+/^-$ anti-PDL1 (control and anti-PD-L1, n=18; abemaciclib and combination, n=19 tumors). Unpaired two-tailed t-tests (a–c,f), one-way ANOVA corrected for multiple comparisons (d, j), two-way ANOVA (g) corrected for multiple comparisons (e,h). Error bars, SD; except (g,j), SEM. *p<0.05, **p<0.01, ***p<0.001, ****p<0.0001. For source data, see Supplementary Table 2.